Geotextiles and Geomembranes xxx (xxxx) xxx

Contents lists available at ScienceDirect

Geotextiles and Geomembranes

journal homepage: www.elsevier.com/locate/geotexmem

Regular Paper

Long-term Performance of Conductive-backed multilayered HDPE Geomembranes

M. Zafari [a], F.B. Abdelaal [b], R. Kerry Rowe [c,*]

[a] GeoEngineering Centre at Queen's-RMC, Queen's University, Kingston, ON, K7L 3N6, Canada
[b] GeoEngineering Centre at Queen's-RMC, Queen's University, Ellis Hall, Kingston, ON, K7L 3N6, Canada
[c] Barrington Batchelor Distinguished University Professor and Canada Research Chair in Geotechnical and Geoenvironmental Engineering, GeoEngineering Centre at Queen's-RMC, Queen's University, Ellis Hall, Kingston, ON, K7L 3N6, Canada

ARTICLE INFO

Keywords:
Geosynthetics
Multilayered textured geomembranes
Conductive-backed geomembranes
White geomembranes
Municipal solid waste landfills
Degradation

ABSTRACT

The long-term performance of three multilayered textured white conductive-backed geomembranes (GMBs) is compared to the comparable textured nonconductive GMBs and their smooth edge/equivalent to investigate the effect of the conductive layer on their longevity. Oven immersion in synthetic municipal solid waste leachate is used at a range of temperatures to accelerate the ageing during an incubation period of 50 months. It is shown that the conductive layer can antagonistically or synergistically affect the antioxidant depletion of conductive-backed GMBs relative to nonconductive GMBs produced by the same GMB manufacturer and formulated using the same nominal resin and antioxidant package. However, their relative degradation at 85 °C does not necessarily follow their relative antioxidant depletion times implying that the manufacturing process and the interaction between the additive packages of these GMBs can affect their relative degradation beyond the antioxidant depletion stage. Arrhenius modelling predicts the antioxidant depletion stage at field temperatures ranging between 180 and 1400 years at 20 °C for two different conductive-backed GMBs produced by two different manufacturers. With such variation in the long-term performance of conductive-backed GMBs currently available in the market, their durability should be investigated before their use in barrier systems to ensure they can meet the required design life of the desired geoenvironmental application.

1. Introduction

Geomembrane (GMB) liners overlying a geosynthetic clay liner (GCL) or compacted clay liner (CCL) are used as part of the barrier system in different geoenvironmental applications to minimize the migration of contaminants to the surrounding environment (Rowe et al., 2004; Rowe 2005, 2020; Koerner 2012; Touze-Foltz et al., 2016; Priyanto et al., 2019). Under the long-term field exposure conditions, high density polyethylene (HDPE) GMBs are susceptible to oxidative degradation that results in the reduction of their mechanical properties (Rowe and Sangam 2002; Hsuan et al., 2008; Scheirs 2009). This may eventually lead to the stress cracking of the GMB liner under sustained field stresses and hence the loss of their hydraulic barrier function (Abdelaal et al., 2014a; Ewais et al., 2014). The oxidative degradation of a GMB typically occurs in three successive stages (Hsuan and Koerner 1998). Stage I ends when the antioxidants deplete and can no longer protect the polymer from oxidation. Stage II is the induction time to the onset of polymer degradation at which oxidation reactions occur without measurable change in the mechanical properties of the GMB. Stage III starts when there is a measurable change in the mechanical properties (e.g., tensile property (ASTM 2020a); melt flow index (ASTM 2013); stress crack resistance (ASTM 2020b)) that eventually leads to nominal failure of the GMB (e.g., a drop to 50% of the initial or specified value of the different GMB properties).

Besides the GMB formulation and exposure conditions that govern a GMB's long-term performance, proper GMB installation associated with construction quality assurance (CQA) is another key factor to achieving the desired hydraulic barrier function of the GMB and hence adequate environmental protection. Thus, it is crucial to ensure the integrity of the GMB liner in the short-term by minimizing the number of installation-induced holes in the GMB during and just after the construction of the facility (Giroud and Bonaparte 1989; Forget et al., 2005; Ng and Zheng 2016; Gilson-Beck 2019). Electrical leak location (ELL) surveys are used as an important part of the CQA to locate holes/defects in the GMB after

* Corresponding author.
E-mail addresses: mohsen.zafari@queensu.ca (M. Zafari), fady.abdelaal@queensu.ca (F.B. Abdelaal), kerry.rowe@queensu.ca (R.K. Rowe).

https://doi.org/10.1016/j.geotexmem.2023.03.007
Received 19 August 2022; Received in revised form 20 March 2023; Accepted 26 March 2023

installation and before the liner goes into service. While there are several ELL methods that can be performed for the bare GMBs or the GMBs covered with soil/water (ASTM 2021), they all involve the basic principle of applying an electric potential across the conductive layers immediately overlying and underlying the electrically nonconductive GMB liner. Thus, the electrical current will only flow through the hydraulically significant holes/defects to cause discontinuities in the electric potential to allow locating these leaks in the installed GMB liner. A key to a successful ELL is the availability of sufficiently conductive materials above and below the GMB with good contact with the GMB, especially at the locations of these defects (ASTM 2021). Thus, the presence of holes at the peak of wrinkles or when the GMB is separated from the conductive subgrade by an insulating secondary liner in double-lined facilities limits the efficiency of locating these leaks using the ELL method (Charpentier and Jacquelin 2018). However, many of these limitations can be overcome when a conductive-backed GMB is used instead of the traditional nonconductive GMB liners.

In general, carbon black is used in the HDPE GMB formulation (2–3% of the total weight) for ultraviolet-radiation screening (Mwila et al., 1994; Hsuan et al., 2008; Rowe and Jefferis 2022). While carbon black is intrinsically electrically conductive (Spahr et al., 2017), when it is added to the GMB formulation, the level of conductivity of the polymer depends on the carbon black properties (i.e., type and size of the particles and their surface chemistry), carbon black concentration, the polymer type, the mixing process, as well as the quality and number of carbon black interparticle contacts (Huang 2002; Pantea et al., 2003; Spahr et al., 2017). To enhance the level of conductivity for the conductive skin relative to the other GMB layers, conductive-backed GMBs are typically produced using separate extruders for the core and conductive layer. The conductive skin is then extruded using a different masterbatch stabilized with the desired type and amount of carbon black to ensure higher electrical conductivity of the conductive bottom skin relative to the core and top surface layers (Messmer and Cadwallader 1994; Scheirs 2009). These GMBs can be coextruded with white pigments in the upper skin to reduce the temperature of the exposed GMB. The outer surfaces of these GMBs can be also textured to increase the interface friction of the barrier system layers. However, introducing different masterbatches in the skin and core layers (different carrier resins and/or stabilizers) to equip these multilayered GMBs with such desirable characteristics provides additional challenges for the assessment of their long-term behaviour relative to the traditional single formulation (i.e., smooth black) GMBs.

The effect of these different functionalized layers on the long-term behaviour of the multilayered GMBs has received relatively little attention in the literature. Zafari et al. (2023) investigated the effect of texturing on the degradation stages of multilayered GMBs by comparing the longevity of two multilayered nonconductive textured white HDPE GMBs to their smooth edges when immersed in simulated municipal solid waste (MSW) leachate at different elevated temperatures over 50 months of ageing. While the two portions of the roll had similar initial properties, the degradation times and behaviour of the textured portion were different from the smooth edges of the two GMBs examined. This difference mainly arose from the manufacturing process of these GMBs resulting in different core thicknesses of the textured portion compared to the smooth edge. Additionally, the effect of such a small difference in core thickness on the relative depletion of antioxidants from the two portions of the roll was not consistent for the two GMBs examined. While this study gave insights into the degradation behaviour of multilayered nonconductive GMBs, it demonstrated the need for examining both portions of the roll to assess the GMB degradation times despite their similar initial properties.

Examining the long-term performance of conductive-backed multilayered GMBs and the effect of the conductive layer is expected to be more complex than multilayered nonconductive GMBs examined by Zafari et al. (2023). This is because the manufacturing process of these GMBs can result in partial or complete removal of the conductive layer at the smooth edge of the roll. Thus, in addition to the thickness difference, the formulation and hence the initial properties can change from the textured portion to the smooth edge. This change in formulation, particularly the carbon black, may antagonistically or synergistically affect the antioxidant depletion of the conductive-backed textured GMB relative to its smooth edge and hence, may also alter the degradation behaviour of the two portions of the roll (Hawkins et al., 1959; Kovács and Wolkober 1976; Mwila et al., 1994; Peña et al. 2000a, 2000b, 2001a, 2001b; Phease et al., 2000; Wong and Hsuan, 2012, 2014, 2016). For example, Phease et al. (2000) observed an increase in the initial oxidative induction time (OIT) value of a medium-density polyethylene resin stabilized with phenolic and phosphite antioxidants when carbon black was added into the polymer formulation. However, Hawkins et al. (1959) showed that the effectiveness of phenol antioxidants in polyethylene was decreased due to the addition of carbon black. Carbon black was also shown to affect the mechanical properties of polyethylene. For instance, Deveci et al. (2018) reported a significant decrease in the tensile break properties of polyethylene pipes with an insufficient carbon black distribution in the polymer matrix. This may also result in the formation of stress concentration spots that may reduce the resistance of the resin to slow crack growth (Gholami et al., 2020). Thus, changing the carbon black type or concentration in the skin layer of conductive-backed GMBs is expected to affect the initial properties and hence the performance of these GMBs relative to nonconductive GMBs even those formulated with similar nominal core resin and antioxidant packages. Thus, the objective of this paper is to fill this knowledge gap by examining the long-term performance of double-sided textured, single-sided textured, and smooth multilayered conductive-backed GMBs and compare their degradation behaviour to nonconductive GMBs produced using the same nominal resin and antioxidant packages.

2. Experimental investigation

2.1. GMBs examined

The six commercially available multilayered HDPE GMBs investigated in this study were manufactured from the same medium density polyethylene nominal resin (Chevron Marlex PE K306) by two different GMB manufacturers in 2017. All six GMBs were coextruded blown film materials with a white layer on the upper skin only. The textured GMBs and their smooth edges/equivalents are designated as xTDs, *xTD*, *xTC*, xTBs, xTB, *yI*, *yTA*, yTB in Tables 1 and 2. The first letter (x or y) denotes the manufacturer of the GMB. Textured GMBs (either single-sided or double-sided) are denoted with the letter "T" while the letter "s" denotes the smooth edge of the textured roll. To easily identify conductive-backed GMBs, their destinations are written in *italic* throughout the paper. The third letter (A, B, and C) distinguishes the GMBs produced by the same manufacturer. The GMBs were divided into two groups based on their manufacturers (Tables 1 and 2) to examine the effect of the conductive layer and texturing on the performance of the GMBs produced by each GMB manufacturer.

Group 1 GMBs includes.

(i) a double-sided textured conductive-backed GMB (denoted by *xTD*),
(ii) a single-sided textured (i.e., textured white surface and smooth conductive bottom layer) conductive-backed GMB (denoted by *xTC*), and
(iii) a double-sided textured nonconductive GMB (denoted by xTB).

A comparison on the degradation behaviour of conductive-backed *xTD* and *xTC* with the nonconductive xTB allows an investigation of the effect of the conductive layer on textured GMBs all produced using the same manufacturer and the same nominal resin.

xTB and *xTD* were produced with smooth edges (denoted generically

Table 1
Initial properties of GMBs: Group 1.

Property	Method	Unit	Mean ± Standard deviation				
GMB designator	–	–	xTDs	*xTD*	*xTC*	xTBs	xTB
Texturing	–	–	Smooth	Double sided	Single sided	Smooth	Double sided
Conductive layer	–	–	No[a]	Yes	Yes	No	No
Core thickness	ASTM D5994	mm	1.75 ± 0.01	2.66 ± 0.09[b]	2.19 ± 0.06[b]	2.0 ± 0.1	2.22 ± 0.02[b]
Asperity height for white layer	ASTM D7466	mm	–	0.77 ± 0.07	0.60 ± 0.08	–	0.59 ± 0.08
Asperity height for bottom layer	ASTM D7466	mm	–	0.49 ± 0.12	–	–	0.69 ± 0.06
Std-OIT (bore-cut)[c]	ASTM D3895	min.	290 ± 20	220 ± 35	245 ± 25	285 ± 4.0	284 ± 4.0
Std-OIT (homogenized)[d]	ASTM D8117	min.	N/A	220 ± 4.0	N/A	315 ± 7.0	300 ± 10
HP-OIT (bore-cut)[d]	ASTM D5885	min.	1460 ± 50	705 ± 50	745 ± 65	1430 ± 25	960 ± 80
HP-OIT (homogenized)[d]	ASTM D5885	min.	N/A	970 ± 70	N/A	1530 ± 70	1550 ± 90
Resin density	ASTM D1505	g/cc	0.937	0.938	0.938	0.937	0.937
GMB density	ASTM D792	g/cc	0.948	0.949	0.949	0.948	0.948
HLMI (21.6 kg)	ASTM D1238	g/10min	15.3 ± 0.5	15.2 ± 0.7	15.2 ± 0.7	15.3 ± 0.5	15.3 ± 0.5
LLMI (2.16 kg)	ASTM D1238	g/10min	0.14	0.14	0.14	0.14	0.14
HLMI/LLMI	ASTM D1238	–	109	109	109	109	109
SCR *(notched from white side)*	ASTM D5397	h	>4000	N/A	1537 ± 415	1630 ± 250	N/A
Tensile properties (Machine direction) results are the average of 10 tests							
Strength at Yield	ASTM D6693 Type IV	kN/m	31 ± 0.5	43 ± 2.0	38 ± 1.0	35 ± 1.0	43 ± 3.0
Strength at Break		kN/m	50 ± 1.0	40 ± 11	44 ± 1.0	56 ± 1.0	44 ± 11
Strain at Yield		%	21 ± 0.5	23 ± 2.0	22 ± 1.0	21 ± 0.6	24 ± 1.0
Strain at Break		%	712 ± 11	470 ± 108	580 ± 14	720 ± 15	536 ± 34
Tensile properties (Cross-machine direction) results are the average of 10 tests							
Strength at Yield	ASTM D6693 Type IV	kN/m	33 ± 0.5	45 ± 3.0	39 ± 1.0	36 ± 1.0	45 ± 1.0
Strength at Break		kN/m	50 ± 1.0	25 ± 14	39 ± 11	51 ± 2.0	35 ± 13
Strain at Yield		%	19 ± 0.3	22 ± 1.0	22 ± 2.0	21 ± 1.0	23 ± 2.0
Strain at Break		%	760 ± 0.0	357 ± 175	571 ± 69	704 ± 26	470 ± 120
Tensile properties (Machine direction) results are the average of 10 tests							
Strength at Yield	ASTM D638 Type V	kN/m	33 ± 1.0	47 ± 4.0	48 ± 1.0	39 ± 2.0	47 ± 3.0
Strength at Break		kN/m	65 ± 3.0	43 ± 9.0	40 ± 12	70 ± 4.0	42 ± 13
Strain at Yield		%	32 ± 1.0	39 ± 4.0	33 ± 2.0	31 ± 1.0	39 ± 2.0
Strain at Break		%	720 ± 7.0	394 ± 18	464 ± 15	728 ± 8	427 ± 18
Tensile properties (Cross-machine direction) results are the average of 10 tests							
Strength at Yield	ASTM D638 Type V	kN/m	36 ± 1.0	48 ± 4.0	49 ± 2.0	40 ± 1.0	45 ± 4.0
Strength at Break		kN/m	71 ± 2.0	35 ± 15	41 ± 5.0	74 ± 4.0	40 ± 11
Strain at Yield		%	30 ± 1.0	38 ± 2.0	32 ± 2.0	29 ± 1.0	38 ± 2.0
Strain at Break		%	800 ± 0.0	326 ± 41	477 ± 9.0	800 ± 7.0	414 ± 34

N/A = Not available.
Strength at break was measured as the load (per unit width) when the specimen actually breaks.
[a] Inspection of the bottom layer using the multimeter showed that it is not conductive.
[b] The nominal thickness provided by manufacturer is 2 mm.
[c] The results are the average of 10 tests.
[d] The resuls are the average of 5 tests.

as xTBs and xTDs, respectively) for welding purposes in the field. These smooth edges had different thicknesses and shades of colour on the white surface from their textured parts. For *xTD*, the measured electrical conductivity was significantly reduced at the smooth edge (xTDs) relative to the textured part implying that the conductive skin could be very thin or absent at the smooth edge of xTDs. Thus, the degradation behaviour of the smooth edges xTBs and xTDs is compared to their textured counterparts to examine the effect of texturing and potential changes in the formulation at the different portions of the multilayered GMB rolls for conductive-backed and nonconductive GMBs.

Group 2 GMBs (denoted generically as *yI*, *yTA*, and yTB) includes.

(i) a smooth conductive-backed GMB (*yI*),
(ii) a double-sided textured conductive-backed GMB (*yTA*), and
(iii) a double-sided textured nonconductive GMB (yTB; Table 2).

Unlike Group 1, *yTA* and yTB were produced with weld-edges that are not completely smooth and thus not suitable for stress crack resistance (SCR) testing (ASTM 2020b; GRI-GM13, 2021). For this reason, *yI* was supplied by the manufacturer as the smooth equivalent to *yTA*. Thus, a comparison of the degradation behaviour of *yI* to *yTA* is used to investigate the effect of texturing on conductive-backed GMBs since this cannot be explored for Group 1 GMBs when comparing *xTD* to xTDs due to the partial/complete removal of the conductive skin of the smooth xTDs.

The performance of *yTA* is also compared to yTB to investigate the potential effect of the conductive layer on the multilayered textured GMBs similar to the comparison of *xTD* and xTB in Group 1 but for two GMBs produced by a different manufacturer to explore the effect of the manufacturing process of conductive-backed GMBs on their long-term performance.

Both manufacturers (i.e., x and y) did not disclose the type and amount of carbon black they used to produce the conductive-backed GMBs. Additionally, the exact thickness of the conductive layer is unknown. However, the visual inspection of the conductive-backed GMBs under the microscope showed that the thickness of the conductive layer is less than the 5% of their total thicknesses.

2.2. Immersion testing

The GMB coupons (190 mm × 100 mm) from all GMBs were immersed in 4-Litre glass jars filled with simulated MSW leachate (denoted as MSW-L3). The MSW-L3 leachate used (TDS ≈ 12,000mg/L; pH ≈ 7; electrical potential Eh ≈ −120 mV) was prepared using distilled

Table 2
Initial properties of GMBs: Group 2.

Property	Method	Unit	Mean ± Standard deviation		
GMB designator	–	–	*yI*	*yTA*	yTB
Texturing	–	–	Smooth	Double sided	Double sided
Conductive layer	–	–	Yes	Yes	No
Core thickness	ASTM D5994	mm	2.38 ± 0.05	2.20 ± 0.06	2.36 ± 0.05
Asperity height for white layer	ASTM D7466	mm	–	0.76 ± 0.07	0.70 ± 0.08
Asperity height for bottom layer	ASTM D7466	mm	–	0.95 ± 0.01	0.45 ± 0.07
Std-OIT (bore-cut)	ASTM D3895	min.	165 ± 3.0	165 ± 20	165 ± 3.0
Std-OIT (homogenized)	ASTM D8117	min.	200 ± 6.0	200 ± 5.0	N/A
HP-OIT (bore-cut)	ASTM D5885	min.	780 ± 15	800 ± 65	915 ± 40
HP-OIT (homogenized)	ASTM D5885	min.	1200 ± 100	1115 ± 90	N/A
Resin density	ASTM D1505	g/cc	0.937	0.937	0.937
GMB density	ASTM D792	g/cc	0.949	0.944	0.945
HLMI (21.6 kg)	ASTM D1238	g/ 10min	12.6 ± 0.3	12 ± 0.2	13.1 ± 0.5
LLMI (2.16 kg)	ASTM D1238	g/ 10min	0.09 ± 0.001	0.09 ± 0.01	0.08 ± 0.002
HLMI/LLMI	ASTM D1238	–	149	120	165
SCR *(notched from white side)*	ASTM D5397	h	1432 ± 370	N/A	N/A
Tensile properties (Machine direction) results are the average of 10 tests					
Strength at Yield	ASTM	kN/m	41 ± 1.0	41 ± 1.0	47 ± 2.0
Strength at Break	D6693	kN/m	75 ± 4.0	25 ± 15	50 ± 14
Strain at Yield	Type IV	%	20 ± 0.5	23 ± 1.0	24 ± 1.0
Strain at Break		%	792 ± 30	305 ± 115	572 ± 50
Tensile properties (Cross-machine direction) results are the average of 10 tests					
Strength at Yield	ASTM	kN/m	43 ± 1.0	41 ± 2.0	47 ± 1.0
Strength at Break	D6693	kN/m	71 ± 8.0	16 ± 3.0	49 ± 6.0
Strain at Yield	Type IV	%	19 ± 0.5	23 ± 1.0	24 ± 1.0
Strain at Break		%	760 ± 68	300 ± 105	552 ± 44
Tensile properties (Machine direction) results are the average of 10 tests					
Strength at Yield	ASTM	kN/m	45 ± 1.0	45 ± 1.0	50 ± 2.0
Strength at Break	D638 Type	kN/m	90 ± 5.0	39 ± 9.0	56 ± 6.0
Strain at Yield	V	%	30 ± 1.0	40 ± 3.0	39 ± 3.0
Strain at Break		%	760 ± 12	354 ± 20	486 ± 15
Tensile properties (Cross-machine direction) results are the average of 10 tests					
Strength at Yield	ASTM	kN/m	47 ± 1.0	45 ± 1.0	51 ± 2.0
Strength at Break	D638 Type	kN/m	95 ± 2.0	33 ± 9.0	48 ± 7.0
Strain at Yield	V	%	28 ± 0.0	38 ± 3.0	39 ± 4.0
Strain at Break		%	792 ± 5.0	342 ± 22	446 ± 8.0

- N/A = Not available.
-Strength at break was measured as the load (per unit width) when the specimen actually breaks.

water mixed with organic/inorganic salts, surfactant, reducing agent, and trace metal solution based on the chemical analysis of a MSW landfill leachate in Ontario, Canada (Rowe et al., 2008; Abdelaal et al., 2014b). The GMB coupons were separated using 5 mm diameter glass rods to ensure the exposure of GMBs to the leachate from both sides. To accelerate the GMB ageing, the immersion tests were conducted at 40, 55, 65, 75, and 85 °C for Group 1 GMBs except for *xTC*, which was only incubated at 85 °C. For Group 2, while the GMBs were immersed using the same temperature range as Group 1, only four temperatures were used (40, 55, 70, and 85 °C) for accelerating ageing to reduce the number of tests required to examine their degradation at different temperatures. To prevent the build up of antioxidants in leachate and to ensure a constant strength during the entire study (Rowe et al., 2008), the MSW-L3 was replaced every 2 months. The samples were extracted at different incubation times to monitor the changes in the GMB properties with time at the different immersion temperatures.

2.3. Index testing

Different ASTM index tests were used to assess the initial properties of the GMBs (Tables 1 and 2) and to monitor their degradation with ageing. Differential scanning calorimetry (DSC) was used to monitor the antioxidant depletion of the GMBs and to quantify the first stage of degradation. The standard oxidative induction time (Std-OIT 200 °C, 35 kPa; ASTM, 2019) was used to detect hindered phenols and phosphites antioxidants while the high pressure oxidative induction time (HP-OIT 150 °C, 3450 k Pa; ASTM 2020c) was conducted to detect thiosynergists and hindered amine [light] stabilizers (HALS also known as HAS) (Hsuan and Koerner, 1998). Bore-cut specimens were used for the OIT tests with the white layer facing up in the DSC during the entire study since the ASTM in 2017 did not require any homogenization of the OIT samples at the time of the initiation of the ageing experiments in 2017.

Due to the recent requirement of sample homogenization for multi-layered GMBs, the effect of homogenization on the OIT depletion of nonconductive and conductive-backed GMBs was examined by testing the homogenized specimens of xTB and *xTD* at different incubation times and comparing the results to the OIT data obtained from the bore-cut method. Although the dispersion of the results was higher in bore-cut method, the results showed that the depletion rates for the homogenized specimens were either similar or slower than those obtained using the bore-cut specimens. For instance, while the initial HP-OIT of the homogenized samples of *xTD* and xTB was 1.4–1.6 fold higher than the values obtained using the bore-cut method, the depletion of the normalized HP-OIT (i.e., HP-OIT at a given time divided by the initial value) followed the same trend for the two testing techniques for both the conductive-backed and nonconductive GMBs (Fig. 1). Thus, predicting the antioxidant depletion time based on the OIT results obtained using the bore-cut specimens should err on the conservative side of prediction for both conductive-backed and nonconductive GMBs. While the effect of homogenization on the prediction of the antioxidant depletion stage warrants a more detailed investigation, this paper only deals with the bore-cut method.

The physical and mechanical properties of the GMB were monitored in terms of melt flow index test (MFI; ASTM, 2013), tensile test (ASTM 2020a), and notched constant tensile load (NCTL) test for stress crack resistance (SCR; ASTM 2020b) to quantify Stages II and III of the GMB degradation stages. In the MFI test, the GMB sample was extruded at 190 °C to assess the changes in molecular weight of the polymer to infer degradation by either cross-linking or chain-scissioning mechanisms (Hsuan and Koerner 1998).

To monitor the change in the tensile break properties with ageing, tensile tests were conducted in both the machine (MD) and cross-machine (XD) directions. Type IV tensile specimens (dog bone specimens; ASTM 2020a) were only used to test the unaged materials while the smaller dog bone Type V specimens (ASTM 2014) were used to monitor the degradation of the aged samples at a displacement rate of 50mm/min. The NCTL test was also used to examine the change in SCR using dog bone specimens cut in the cross-machine direction. The SCR of the double-sided textured *xTD*, xTB, and *yTA* was obtained by testing the smooth edges (i.e., xTDs and xTBs) or the smooth equivalent GMB made from the same formulation of the textured GMB (i.e., *yI* for *yTA*) with specimens notched on the white side (ASTM 2020b). For *xTC* with a single textured surface, the specimens were notched on the white textured layer to maintain a constant ligament of 80% of the GMB nominal thickness in all the specimens examined by removing the effect of the thickness variability at the textured side. The unaged and aged

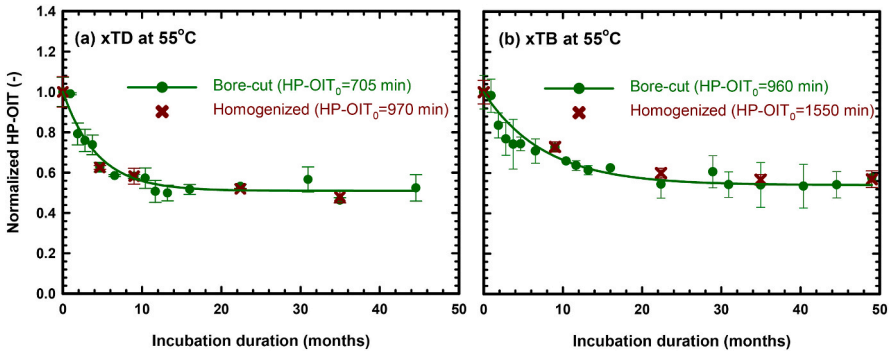

Fig. 1. Comparison of normalized rate of OIT depletion using both bore-cut and homogenized specimens for (a) conductive-backed *xTD* and (b) nonconductive xTB.

specimens were then immersed in 10% IGEPAL solution at 50 °C under applied stress representing 30% of the yield strength measured for the as manufactured (i.e., including all functionalized layers) unaged specimens of xTDs, xTBs, *yI*, and *xTC*.

3. Results and discussion

3.1. Initial OIT values

Although all the GMBs examined were manufactured using the same nominal resin, the different additives and formulations of their outer skins resulted in the variation of their initial OIT values (Tables 1 and 2). For Group 1 GMBs, while the initial Std-OIT (Std-OIT_0) of the nonconductive xTB was similar to its smooth edge, the initial HP-OIT (HP-OIT_0) of the smooth xTBs (1430 ± 25min) was 1.5 times higher than the HP-OIT_0 of xTB (960 ± 80min). However, the HP-OIT_0 of the homogenized specimens of xTB (1550 ± 90min) and xTBs (1530 ± 70min) were similar. This suggests that the difference in the HP-OIT_0 of the bore-cut specimens between the textured portion and the smooth edge could be due to the initial variation of the concentration of the high molecular weight antioxidants across the GMB layers that was manifested due to the use of the bore-cut method. Thus, texturing and the difference in the thickness of the skin layers between the textured and smooth parts of the nonconductive xTB had minor effects on the initial Std-OIT and HP-OIT values.

For the conductive-backed GMBs, texturing also had a minor effect on the initial OIT values given the statistically insignificant difference in the Std-OIT_0 and HP-OIT_0 of the conductive-backed double-sided textured *xTD* and the single-sided textured *xTC*. For the effect of the conductive layer, while the smooth edges xTDs and xTBs were initially formulated with the same concentration of antioxidants (as implied from their similar Std-OIT_0 and HP-OIT_0), the nonconductive xTB had a similar initial OIT to its smooth edge xTBs, whereas the textured *xTD* had 24% lower Std-OIT_0 and 52% lower HP-OIT_0 relative to its smooth edge xTDs. Such difference in the initial OIT values between the textured and smooth edge of the conductive-backed GMB can be attributed to the difference in the conductive layer thickness between *xTD* and xTDs. This implies that the thicker conductive skin at the textured part could have had an antagonistic interaction with the antioxidants resulting in lower Std-OIT_0 and HP-OIT_0 values than at the smooth edge. Thus, for Group 1 GMBs, the conductive layer affected the initial OIT values.

Unlike Group 1 GMBs, the difference in the Std-OIT_0 and HP-OIT_0 of the conductive-backed and nonconductive GMBs in Group 2 was insignificant (at 95% confidence level) since adding the conductive layer in *yTA* and *yI* did not affect the initial OIT values relative to the nonconductive yTB. Another difference between the conductive-backed *xTD* and *yTA* can also be observed from the comparison of their DSC thermograms to their nonconductive counterparts (Fig. 2). Multiple exothermic peaks were only observed for *xTD*'s bore-cut specimens during the Std-OIT test. This could arise from the different formulation, additives, and oxidation rates of the conductive and nonconductive layers in *xTD* causing such inhomogeneity in the bore-cut OIT specimens (Scheirs et al., 2020) since the homogenized specimens of the same GMB only showed a single exothermic peak during the OIT tests (Fig. 2). To interpret the OIT curves of the bore-cut specimens with multiple exothermic peaks, the last slope of the curve was selected since it consistently gave the closest OIT values to those obtained from homogenization method. For Group 2 GMBs, the conductive *yTA* and the nonconductive yTB showed a single peak thermogram during the Std-OIT tests for both the bore-cut and the homogenized specimens with similar initial OIT values. Thus, unlike *xTD*, the conductive layer of *yTA* did not affect the initial OIT values and the homogeneity of the OIT specimens. This shows that the different formulations (i.e., conductive masterbatch added to the base resin) used by the different GMB manufacturers may have different effects on the initial OIT values of conductive-backed GMBs.

The homogenized specimens of *xTD* had Std-OIT_0 (220 ± 4min; CoV = 2%), which were similar to the bore-cut values (220 ± 35min; CoV = 16%), a greater variation in the results was observed for the bore-cut specimens than the homogenized specimens. Std-OIT_0 of the bore-cut

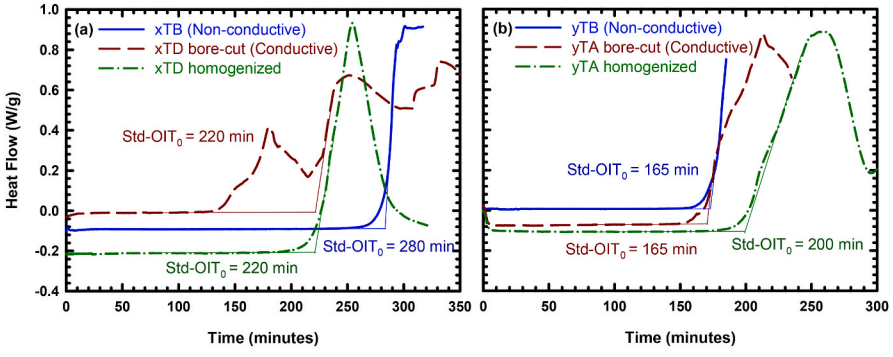

Fig. 2. DSC thermograms for (a) xTB with single peak and *xTD* with multiple peaks; (b) yTB and *yTA* with single peaks.

yTA specimens (165 ± 20min) also had a higher CoV than the homogenized specimens (200 ± 5min) with the homogenized average value being 1.2-fold greater than for the bore-cut specimens. Thus, while using bore-cut method increased the variability in the results (i.e., increased the dispersion of the results compared to homogenization method), the Std-OIT$_0$ of the bore-cut specimens was either similar or lower than those obtained by using homogenization.

3.2. Antioxidant depletion

3.2.1. Std-OIT depletion

For Group 1 GMBs, the Std-OIT for xTDs and xTB depleted to very low residual values (i.e., less than 5min) with single rates (Fig. 3a and b) and hence their Std-OIT depletion was modelled using a first-order (two-parameter) exponential decay function (Hsuan and Koerner 1998; Sangam and Rowe 2002; Rowe et al., 2009; Abdelaal et al., 2014b) given by:

$$OIT_t = OIT_0\, e^{-st} \tag{1}$$

where OIT_t (min) is the OIT value at time t, s (month^{-1}) is the antioxidant depletion rate, and OIT_o (min) is the initial OIT value.

The conductive-backed *xTD* and *xTC* showed a very rapid early Std-OIT depletion rate followed by a slower depletion rate before reaching very low residual values (Fig. 3a and b). Since the traditional two-parameter model (Eq. (1)) cannot capture both the early-time and later-time depletions of *xTD* and *xTC*, their Std-OIT results were fitted by the superposition of two exponential decay functions (Mueller and Jakob 2003; Abdelaal and Rowe 2014; Wong and Hsuan 2016; Rowe et al., 2020) given by:

$$OIT_t = a\, e^{-s_1 t} + b\, e^{-s_2 t} \tag{2}$$

where s_1 (month^{-1}) is the first antioxidant depletion rate, s_2 (month^{-1}) is the second antioxidant depletion rate, and a and b are the exponential fit parameters where $a + b = OIT_o$.

At 85 °C, the Std-OIT depleted to a very low residual value after 6 months for xTDs and xTB, 10 months for *xTD*, and 11 months for *xTC* (Fig. 3a; Table 3). Therefore, despite the rapid early-stage depletion for the conductive-backed GMBs, *xTD* and *xTC* showed longer Std-OIT depletion times at 85 °C compared to the nonconductive xTDs and xTB. The early-stage depletion rate that predominately captures the depletion of antioxidants that are more readily extracted from the GMB (Abdelaal and Rowe 2017), was faster for *xTC* than *xTD*. However, the late-stage depletion rate that dominates the time to depletion (Abdelaal and Rowe 2014) was faster for *xTD* resulting in a shorter depletion time for the double-sided textured GMB compared to the single-sided textured GMB that can be attributed to the higher surface area exposed to the solution for *xTD* than *xTC*. At temperatures below 85 °C, the relative performance of Group 1 GMBs changed with decreasing temperatures. For instance, at 55 °C, xTB reached higher normalized Std-OIT value (22%) than *xTD* (13%) by the end of the 50-month incubation period considered here (Fig. 3b). These results show that the differences in the bottom layer of *xTD* compared to xTDs and xTB may have affected the relative depletion of antioxidants at different temperatures.

For Group 2 GMBs, the conductive-backed and nonconductive GMBs showed similar Std-OIT depletion pattern in which the data depleted to very low residual values with single rates (Fig. 3c and d; Table 4) and hence were fitted using a two-parameter model (Eq. (1)). The observed antioxidant depletion rates (in month^{-1}) for the three GMBs (*yI*, *yTA*, yTB) were (0.004, 0.0045, 0.006) at 40 °C, (0.027, 0.032, 0.055) at 55 °C, (0.22, 0.24, 0.34) at 70 °C, and (0.75, 0.76, 1.1) at 85 °C. Thus, despite the similar initial Std-OIT values, the nonconductive textured GMB, yTB, depleted faster than the conductive-backed textured GMB, *yTA*, with an average factor of 1.5 at all immersion temperatures.

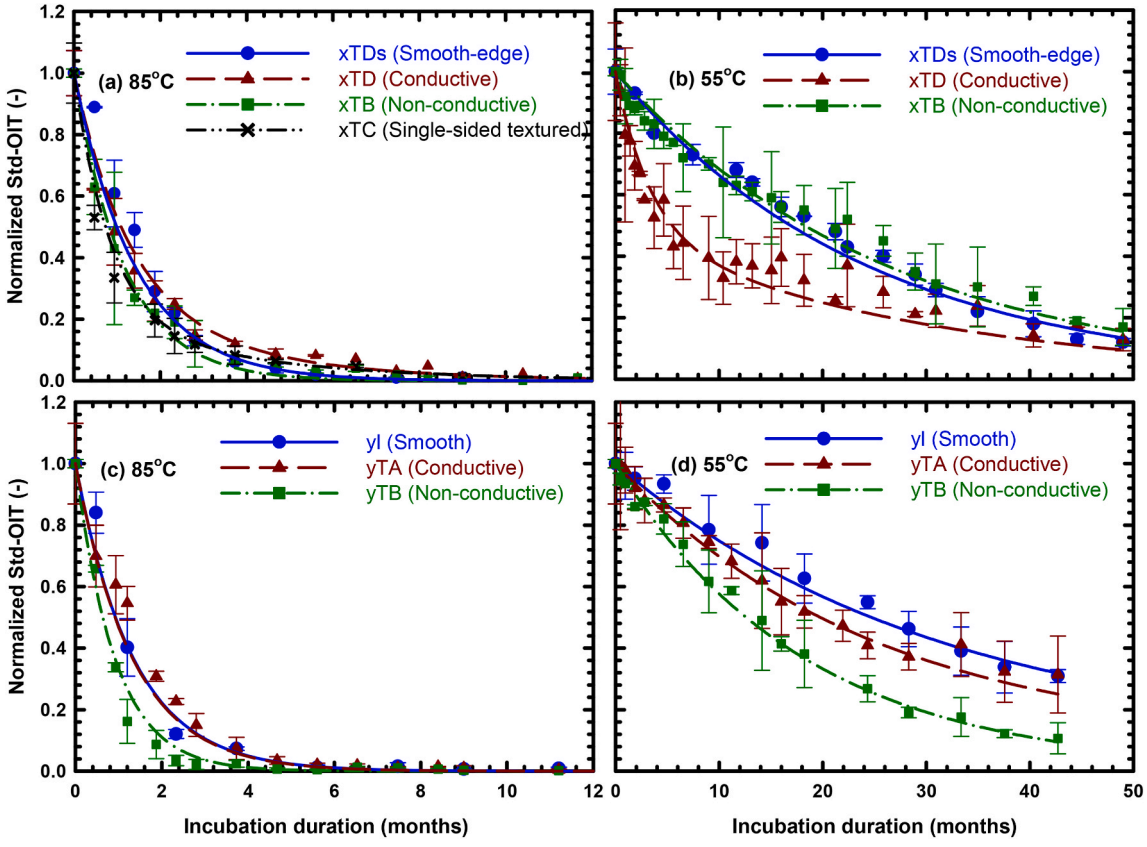

Fig. 3. Variation of normalized Std-OIT (OIT_t/OIT_0) with time in MSW-L3 for (a) xTDs, *xTD*, xTB, and *xTC* at 85 °C; (b) xTDs, *xTD*, and xTB at 55 °C; (c) *yI*, *yTA*, and yTB at 85 °C; (d) *yI*, *yTA*, and yTB at 55 °C.

Table 3
Equations used for fitting Std-OIT and HP-OIT depletions: Group 1.

Temperature (°C)	Equations used for fitting Std-OIT depletion			
	xTDs	*xTD*	xTB	*xTC*
85	$\text{Std-OIT}_t = 290e^{-0.7t}$	$\text{Std-OIT}_t = 160e^{-0.8t} + 60e^{-0.32t}$	$\text{Std-OIT}_t = 285e^{-0.85t}$	$\text{Std-OIT}_t = 194e^{-1.21t} + 51e^{-0.27t}$
75	$\text{Std-OIT}_t = 290e^{-0.37t}$	$\text{Std-OIT}_t = 140e^{-0.6t} + 80e^{-0.15t}$	$\text{Std-OIT}_t = 285e^{-0.3t}$	–
65	$\text{Std-OIT}_t = 290e^{-0.13t}$	$\text{Std-OIT}_t = 130e^{-0.49t} + 90e^{-0.075t}$	$\text{Std-OIT}_t = 285e^{-0.15t}$	–
55	$\text{Std-OIT}_t = 290e^{-0.04t}$	$\text{Std-OIT}_t = 105e^{-0.3t} + 115e^{-0.033t}$	$\text{Std-OIT}_t = 285e^{-0.036t}$	–
40	$\text{Std-OIT}_t = 290e^{-0.004t}$	$\text{Std-OIT}_t = 85e^{-0.2t} + 135e^{-0.014t}$	$\text{Std-OIT}_t = 285e^{-0.004t}$	–
Equations used for fitting HP-OIT depletion				
85	$\text{HP-OIT}_t = 1264e^{-0.30t} + 196$	$\text{HP-OIT}_t = 541e^{-0.42t} + 164$	$\text{HP-OIT}_t = 783e^{-0.27t} + 177$	$\text{HP-OIT}_t = 595e^{-0.33t} + 150$
75	$\text{HP-OIT}_t = 1184e^{-0.24t} + 276$	$\text{HP-OIT}_t = 513e^{-0.32t} + 192$	$\text{HP-OIT}_t = 727e^{-0.21t} + 233$	–
65	$\text{HP-OIT}_t = 1128e^{-0.18t} + 332$	$\text{HP-OIT}_t = 443e^{-0.28t} + 262$	$\text{HP-OIT}_t = 639e^{-0.16t} + 321$	–
55	$\text{HP-OIT}_t = 934e^{-0.14t} + 526$	$\text{HP-OIT}_t = 342e^{-0.23t} + 363$	$\text{HP-OIT}_t = 440e^{-0.13t} + 520$	–
40	$\text{HP-OIT}_t = 711e^{-0.11t} + 749$	$\text{HP-OIT}_t = 200e^{-0.17t} + 505$	$\text{HP-OIT}_t = 217e^{-0.1t} + 743$	–

Table 4
Equations used for fitting Std-OIT and HP-OIT depletions: Group 2.

Temperature (°C)	Equations used for fitting Std-OIT depletion		
	yI	*yTA*	yTB
85	$\text{Std-OIT}_t = 165e^{-0.75t}$	$\text{Std-OIT}_t = 165e^{-0.76t}$	$\text{Std-OIT}_t = 165e^{-1.1t}$
70	$\text{Std-OIT}_t = 165e^{-0.22t}$	$\text{Std-OIT}_t = 165e^{-0.24t}$	$\text{Std-OIT}_t = 165e^{-0.34t}$
55	$\text{Std-OIT}_t = 165e^{-0.027t}$	$\text{Std-OIT}_t = 165e^{-0.032t}$	$\text{Std-OIT}_t = 165e^{-0.055t}$
40	$\text{Std-OIT}_t = 165e^{-0.004t}$	$\text{Std-OIT}_t = 165e^{-0.0045t}$	$\text{Std-OIT}_t = 165e^{-0.006t}$
Equations used for fitting HP-OIT depletion			
85	$\text{HP-OIT}_t = 494e^{-0.27t} + 286$	$\text{HP-OIT}_t = 506e^{-0.28t} + 294$	$\text{HP-OIT}_t = 341e^{-0.33t} + 574$
70	$\text{HP-OIT}_t = 366e^{-0.21t} + 414$	$\text{HP-OIT}_t = 388e^{-0.2t} + 412$	$\text{HP-OIT}_t = 261e^{-0.22t} + 654$
55	$\text{HP-OIT}_t = 217e^{-0.11t} + 563$	$\text{HP-OIT}_t = 242e^{-0.11t} + 558$	$\text{HP-OIT}_t = 166e^{-0.15t} + 749$
40	$\text{HP-OIT}_t = 134e^{-0.069t} + 646$	$\text{HP-OIT}_t = 113e^{-0.072t} + 687$	$\text{HP-OIT}_t = 77e^{-0.08t} + 838$

Although yTB had higher thickness and lower asperity height than *yTA* that should reduce the rate of Std-OIT depletion (Zafari et al., 2023), the faster depletion of the nonconductive GMB suggests that adding the conductive layer retarded the Std-OIT depletion of *yTA* relative to yTB. In addition, the conductive-backed GMBs (i.e., *yTA* and *yI*) showed very similar Std-OIT depletion behaviour at different immersion temperatures with slightly faster depletion rates for the textured GMB. The faster depletion of *yTA* can be attributed to its lower core thickness and larger surface area exposed to leachate compared to *yI* that could increase the leaching and migration of antioxidants from the surface (Morsy and Rowe 2019; Zafari et al., 2023).

In summary, both texturing and adding the conductive layer affected the Std-OIT depletion of the two groups of GMBs produced by different manufacturers. For the texturing effect, the conductive-backed textured *xTD* and *yTA* depleted slightly faster than the conductive-backed single-sided textured *xTC* and the smooth *yI*, respectively, and hence, texturing increased the rate of antioxidant depletion. The effect of texturing (i.e., increasing the surface area exposed to leachate) for Group 1 GMBs surpassed the effect of the GMB thickness on the relative antioxidant depletion since *xTD* has a greater thickness than *xTC* whereas, in Group 2 GMBs, both texturing and the lower thickness of *yTA* resulted in its faster antioxidant depletion relative to *yI*. Although it is difficult to draw a definitive conclusion regarding the effect of adding the conductive layer without knowing the exact type and amount of carbon black used in the formulation of the core and conductive layer, and further investigation of the effect of the carbon black in the conductive layer relative to the core would be useful, the difference in the relative performance of conductive-backed and nonconductive GMBs between Groups 1 and 2 suggests that the conductive layer can antagonistically (e.g., Group 1 GMBs at lower temperatures) or synergistically (e.g., Group 2 GMBs at all temperatures and Group 1 GMBs at 85 °C) affect the rate of antioxidant depletion depending on the manufacturing process and the additive package used in the formulation of the GMB. This can be attributed to the effects of adding more and/or different carbon black on the antioxidant depletion of HDPE GMBs (Hawkins et al., 1959; Phease et al., 2000; Wong and Hsuan 2016). However, for both groups, adding the conductive layer had a higher impact on the antioxidant depletion than texturing the surfaces. For instance, for Group 2 GMBs at 55 °C, the difference in the rates of Std-OIT depletion was 18% between *yI* and *yTA* and 70% between *yTA* and yTB. The higher effect of adding the conductive layer than texturing the surfaces on the antioxidant depletion implies that the interaction of the antioxidants with the carbon black added to the conductive layer had a greater effect on the antioxidant depletion than increasing the surface area exposed to the solution.

3.2.2. HP-OIT depletion

The HP-OIT of the GMBs with suspected high molecular weight HALS, depleted to high residual values (Fig. 4) and hence a three-parameter exponential decay function was used to fit the data viz:

$$OIT_t = \left[(OIT_0 - OIT_r)e^{-st}\right] + OIT_r \quad (3)$$

where OIT_t (min) is the OIT value at time t, s (month^{-1}) is the antioxidant depletion rate, OIT_0 (min) is the initial OIT value, and OIT_r (min) is the residual OIT value.

Previous studies (e.g., Morsy and Rowe 2019; Zafari et al., 2023) showed that texturing has a minor effect on the HP-OIT depletion rates due to the high resistance of the high molecular antioxidants to depletion by leaching and extraction. However, different HP-OIT depletion rates and residual values at the different immersion temperatures were observed for the conductive-backed and nonconductive GMBs examined (Tables 3 and 4).

For Group 1 GMBs, the normalized residual values (i.e., the residual value divided by the initial value) for the conductive-backed and nonconductive GMBs (*xTD*, xTB) were (0.72, 0.77) at 40 °C, (0.51, 0.54) at 55 °C, (0.37, 0.33) at 65 °C, (0.27, 0.24) at 75 °C, and (0.23, 0.18) at 85 °C. While this shows a relatively small difference between the normalized residual values (less than 5%) of the conductive-backed and nonconductive GMBs, the absolute residual values at different temperatures were, on average, 28% lower for *xTD* than xTB due to the difference between their initial HP-OIT$_0$ values (Table 3). Additionally, xTD had consistently faster depletion rates than xTB at all temperatures. For instance, at 55 °C, the observed depletion rates and residual values were, respectively, 0.13 month^{-1} and 520min for xTB and 0.23 month^{-1} and 363min for *xTD*. This difference was not related to the testing method since the homogenized samples gave residual values of 880 ± 36min (57% of the initial value) for xTB and 470 ± 20min (48% of the initial value) for *xTD* that was reached at a faster rate than xTB. Thus, faster depletion of the HP-OIT to the lower absolute residual values was

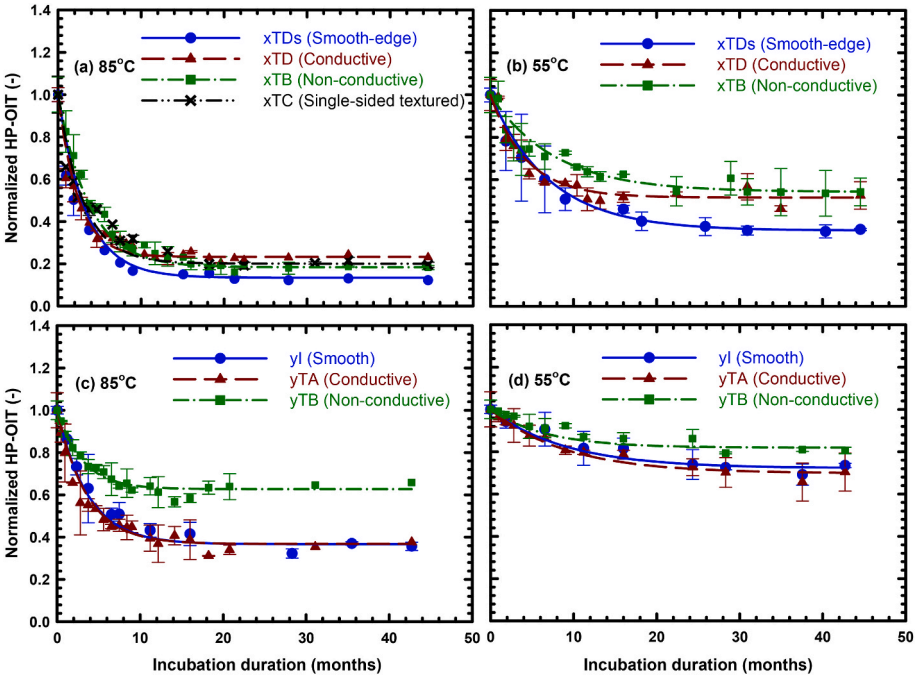

Fig. 4. Variation of normalized HP-OIT (OIT_t/OIT_0) with time in MSW-L3 for (a) xTDs, *xTD*, xTB, and *xTC* at 85 °C; (b) xTDs, *xTD*, and xTB at 55 °C; (c) *yI*, *yTA*, and yTB at 85 °C; (d) *yI*, *yTA*, and yTB at 55 °C.

observed for conductive-backed *xTD* relative to nonconductive xTB.

For the relative depletion of the smooth edge xTDs and the double-sided textured *xTD*, the normalized residual values at different temperatures were lower for xTDs than *xTD* due to the higher initial HP-OIT_0 value of xTDs (1460min vs. 705min). However, xTDs had higher absolute residual values and slower depletion rates than *xTD* at all temperatures (Table 3). This difference between the depletion of *xTD* and xTDs can be attributed to the difference in their conductive bottom layers. The conductive layer in *xTD* resulted in faster depletion of the HP-OIT to the lower absolute residual values for *xTD* relative to xTDs and xTB.

The effect of the conductive layer on the HP-OIT depletion of Group 2 GMBs was different from the behaviour observed for Group 1. With a statistically insignificant difference in the initial HP-OIT_0 values, the nonconductive yTB depleted to significantly higher residual values at different temperatures compared to the conductive-backed GMBs *yTA* and *yI* (Fig. 4c and d; Table 4). The observed depletion rates (in $month^{-1}$) for (*yI*, *yTA*, yTB) were (0.069, 0.072, 0.08) at 40 °C, (0.11, 0.11, 0.15) at 55 °C, (0.21, 0.2, 0.22) at 70 °C, and (0.27, 0.28, 0.33) at 85 °C. Thus, while the small difference between the results can be due to the normal variability of the HP-OIT measured based on bore-cut method, the depletion rates of yTB at different temperatures were, on average, 1.2 times faster than *yI* and *yTA* with relatively similar depletion rates. Therefore, like Std-OIT depletion, opposite trends were observed for the HP-OIT depletion of the conductive-backed GMBs relative to their comparable nonconductive GMBs since the antioxidants were detected by HP-OIT of *xTD* depleted faster than xTB while those of *yTA* depleted slower than yTB. In addition, consistent with previous studies (Morsy and Rowe 2019; Zafari et al., 2023), *yI* and *yTA* showed very similar HP-OIT depletion trend that implies that the thickness and texturing of the outer surfaces did not have an effect on the HP-OIT depletion rates and residual values.

3.2.3. Antioxidant depletion stage prediction

Arrhenius modelling (Koerner et al., 1992) was used to predict the rate of antioxidant depletion at different temperatures using the depletion rates obtained experimentally for Std-OIT and HP-OIT. The Arrhenius equation can be written as:

$$s = Ae^{-(E_a/RT)} \tag{4}$$

where s ($month^{-1}$) is depletion rate, A is the collision factor ($month^{-1}$), E_a is the activation energy for antioxidant depletion (J/mol), R is the universal gas constant (8.314 J/(mol.K)), and T is the absolute temperature (K). Taking the natural logarithm on both sides of Eq. (3) gives:

$$\ln(s) = \ln(A) - \left(\frac{E_a}{R}\right)\left(\frac{1}{T}\right) \tag{5}$$

For the Std-OIT depletion, the parameters A and E_a were estimated for the GMBs exhibited single depletion rates (i.e., xTDs, xTB, *yI*, *yTA*, and yTB) by plotting the natural logarithm of depletion rates at different immersion temperatures against the inverse of absolute temperatures (Fig. 5). For *xTD*, the prediction of Std-OIT depletion time required both the early-time and later-time depletion rates as well as the exponential fit parameters to substitute in Eq. (2). Thus, an Arrhenius plot was established for each of the two rates (s_1 and s_2) by using the experimental data to predict the depletion rates at various temperatures (Fig. 6a). For the exponential fit parameters (a and b), their values that were obtained from fitting Eq. (2) to the experimental data at temperatures between 40 and 85 °C varied linearly with the temperature as observed in previous studies (e.g., Abdelaal and Rowe 2014, 2017). Hence, a and b values at a given temperature (in °C) were estimated from these linear relationships established using the experimental data (Fig. 6b).

The times to Std-OIT depletion for the GMBs were predicted at temperatures between 10 and 85 °C based on 50 months of ageing using an average Std-OIT residual value of 1.5min (Table 5). Two factors affected the accuracy of the predictions and hence, qualifying the relative performance of the GMBs examined. The first factor is the immersion temperature range used to establish the Arrhenius plot. The effect of this factor was clear, especially for Group 1 GMBs in which *xTD* had the longest antioxidant depletion times at 65, 75, and 85 °C but the shortest depletion times at temperatures below 65 °C (this was also confirmed by testing homogenized specimens from xTB and *xTD* at 55 and 85 °C at different incubation times). When all temperatures between 40 and 85 °C were used in establishing the Arrhenius plots, the predicted time

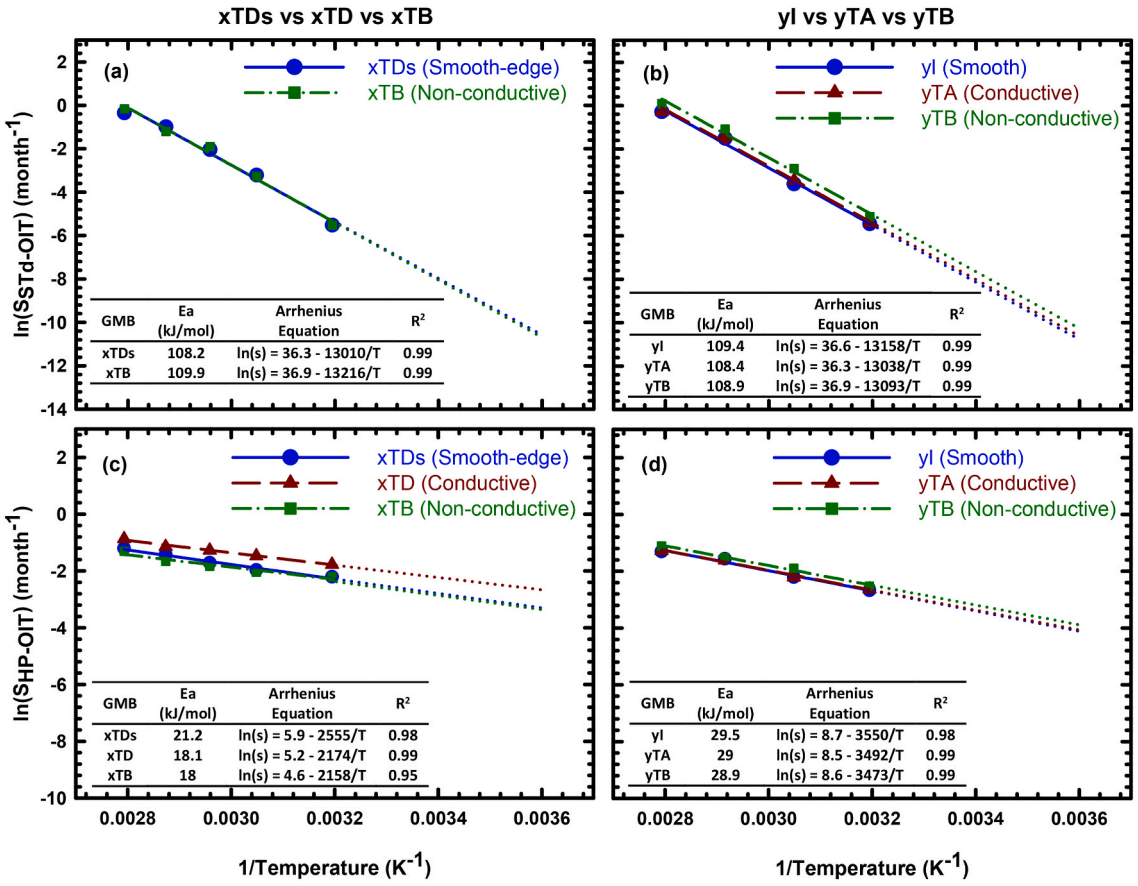

Fig. 5. Arrhenius plots in MSW-L3 for (a) xTDs and xTB based on Std-OIT depletion; (b) *yI*, *yTA*, and yTB based on Std-OIT depletion; (c) xTDs, *xTD*, and xTB based on HP-OIT depletion; (d) *yI*, *yTA*, and yTB based on HP-OIT depletion.

for antioxidant depletion at 40 °C was 85 years for xTDs, 30 years for *xTD*, and 90 years for xTB. This implies that the relative depletion of these GMBs was affected by temperature in which the conductive-backed *xTD* had the lowest resistance to depletion at lower temperatures which was consistent with the experimental data. However, if the Arrhenius plots were established using the depletion rates obtained only at 65, 75, and 85 °C, the antioxidant depletion times at 40 °C were 35, 40, and 37 years for xTDs, *xTD*, and xTB, respectively, showing the minor effect of the conductive layer on the antioxidant depletion times for Group 1 GMBs. This highlights the importance of using lower immersion temperatures (e.g., 40 or 55 °C) together with higher temperatures where the full depletion of antioxidants can be obtained relatively fast for monitoring the degradation behaviour of different GMBs, especially for the geoenvironmental applications with low service temperature.

For Group 2 GMBs, the relative depletion of the GMBs did not change with decreasing temperature. In this case, although the temperature range used to establish the Arrhenius plot slightly affected the predicted depletion times, it had no effect on the relative performance of the GMBs at lower field temperatures. Thus, regardless of the temperature range used for the Arrhenius plot, *yI* had the longest Stage I, followed by *yTA*, and then yTB.

The second factor that controls the accuracy of the predictions is the duration of the immersion tests used to establish the depletion rates at different temperatures. To deduce the effect of this factor, the current data established based on 50 months of ageing were compared to the predictions reported for *xTD*, xTB, *yTA*, and yTB by Rowe et al. (2020) based only on 9–16 months of data. Although the relative performance of the conductive-backed and nonconductive GMBs in both groups was consistent between the current study and Rowe et al. (2020) showing shorter depletion times for *xTD* than xTB and longer depletion times for *yTA* than yTB, the predicted times to depletion based on 50 months of data at lower temperatures were longer than those predicted based on 9–16 months only (Table 5). The increase in the predicted depletion times at lower temperatures by extending the incubation period can be attributed to slower later time depletion of the Std-OIT than the early time depletion that captures the depletion of the antioxidants that are more readily extracted from the GMB. In addition, the difference in the depletion times between the current and Rowe et al. (2020) studies was more significant for the conductive-backed than the nonconductive GMBs due to the complexity of the depletion behaviour of the conductive-backed GMBs (e.g., higher early-time depletion rates than the later-time depletion rates for *xTD*). For instance, at temperatures at or below 40 °C, the current predictions for *xTD* and *yTA* were, respectively, 2 and 4 times higher than the predictions reported by Rowe et al. (2020) using 16 months of data for *xTD* and 9 months for *yTA*. Therefore, while better estimation of Std-OIT behaviour and Stage I duration can establish by a longer incubation period, shorter incubation times resulted in conservative (i.e., shorter) estimates of Stage I duration.

Considering all depletion rates established between 40 and 85 °C during the 50 months of ageing, the current predictions show a different effect of the conductive layer on the duration of Stage I for Group 1 and Group 2 GMBs. For instance, at 20 °C, the predicted Std-OIT depletion time for the conductive-backed GMB, *xTD*, was only 180 years versus 1700 years for the nonconductive GMB, xTB (this difference was not related to the different equations used to model their Std-OIT results since the difference increased when a first-order exponential decay function (Eq. (1)) was used to model the Std-OIT depletion of *xTD*; Abdelaal and Rowe, 2014), while Stage I durations of *yTA* and yTB were 1400 and 970 years, respectively. Again, this highlights the role of the

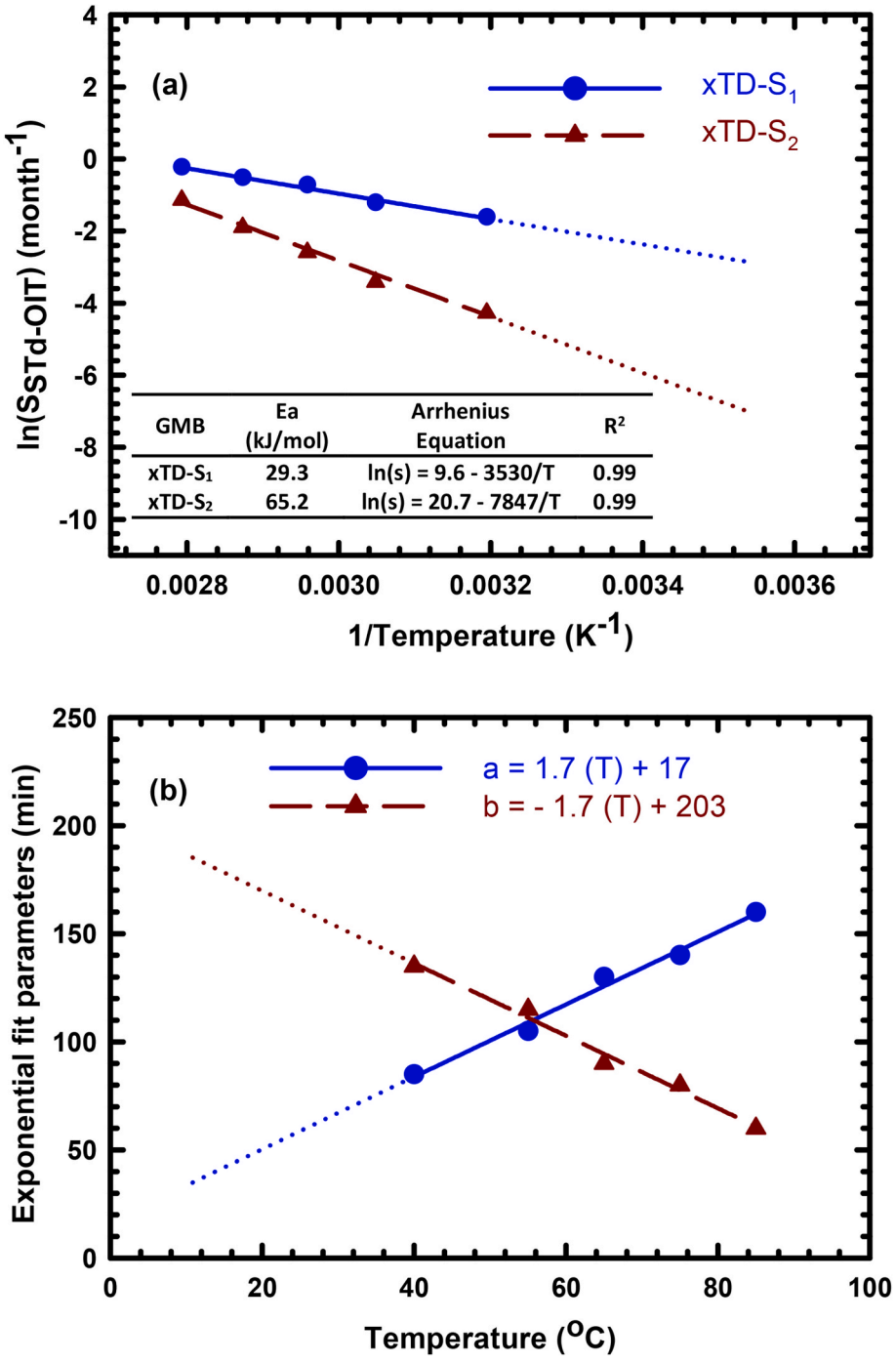

Fig. 6. Std-OIT predictions for the 4-parameter model of *xTD* in MSW-L3: (a) Arrhenius plots of s_1 and s_2; (b) Exponential fit parameters (*a* & *b*).

additives used in the different GMBs by different manufacturers to equip the GMB with electrical conductivity on their longevity. In addition, the predicted duration of Stage I for the smooth edge/equivalent of the conductive-backed textured GMBs were 1600 and 1500 years for xTDs and *yI*, respectively, showing that the conductive-backed textured GMBs in both groups had shorter times to depletion at lower field temperatures relative to their smooth edge/equivalent GMBs. This highlights the importance of assessing the antioxidant depletion times from both portions of the multilayered textured GMB rolls manufactured with the smooth edge given that both parts of the roll are exposed to a solution in the field.

For HP-OIT, prediction of antioxidant depletion time required both the depletion rates and residual values to substitute in Eq. (3). HP-OIT$_r$ was predicted by fitting the experimentally obtained residual values reached after 50 months as indicated in Fig. 7. Then, the HP-OIT depletion times were predicted at temperatures between 10 and 85 °C (Table 6) using the depletion rates and residual values estimated from Figs. 5 and 7. For instance, at 20 °C, the HP-OIT depletion times (in years) for the Group 1 GMBs (xTDs, *xTD*, xTB) were (5.8, 2.6, 3.9) and for Group 2 GMBs (*yI*, *yTA*, yTB) were (6.4, 6.2, 4.9), respectively. Thus, although the difference in the HP-OIT depletion times of the smooth and textured GMBs (i.e., conductive-backed *yI* vs. *yTA*) was very small, adding the conductive layer resulted in an almost 50% and 30% difference in the depletion times of conductive-backed and nonconductive textured GMBs (i.e., *xTD* vs. xTB and *yTA* vs. yTB) in Groups 1 and 2, respectively. However, the effect of adding the conductive layer on the

Table 5
Predicted time to Std-OIT depletion (years); rounded to one significant digit.

Temp. (°C)	Predicted Std-OIT depletion time (years)									
	xTDs	*xTD*		xTB		*yI*	*yTA*		yTB	
	Current[c]	Rowe et al. (2020)[a]	Current[c]	Rowe et al. (2020)[a]	Current[c]	Current[d]	Rowe et al. (2020)[b]	Current[d]	Rowe et al. (2020)[b]	Current[d]
10	>2000	125	470	>2000	>2000	>2000	890	>2000	>2000	>2000
15	>2000	80	280	1900	>2000	>2000	480	>2000	1300	>2000
20	1500	50	180	920	1700	1590	260	1400	630	970
25	700	35	110	460	800	750	145	660	305	450
30	340	25	70	235	370	360	80	320	150	220
35	170	16	45	125	180	180	50	160	80	110
40	85	11	30	65	90	90	30	80	40	55
45	45	7	20	35	47	46	17	42	22	29
50	24	5	13	30	25	24	9	22	12	15
55	13	3.6	9	11	13	13	6.3	12	6.4	8
65	4.1	1.8	4.2	4	4	4	2.5	3.7	2	2.5
70	2.3	1.3	2.9	2.3	2.3	2.3	1.6	2.1	1.2	1.4
75	1.3	0.9	2	1.4	1.4	1.3	1.1	1.2	0.7	0.8
85	0.5	0.5	0.9	0.5	0.5	0.5	0.5	0.4	0.3	0.3

-Time to Std-OIT depletion assessed based on reaching a residual Std-OIT value of 1.5min.
[a] Based on 16 months data.
[b] Based on 9 months data.
[c] Based on 50 months data.
[d] Based on 48 months data.

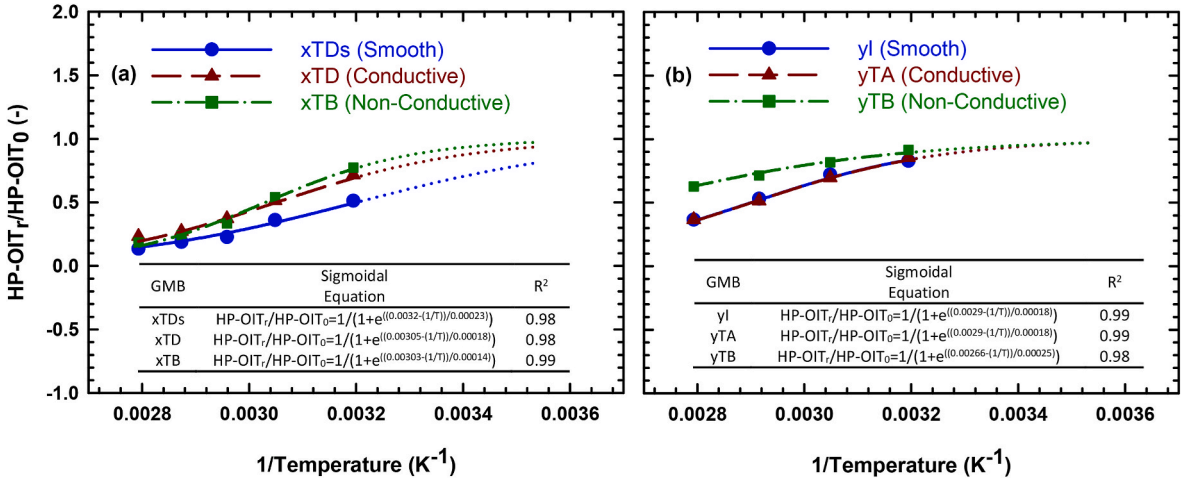

Fig. 7. Plots for residual HP-OIT values versus the incubation temperatures in MSW-L3 for (a) xTDs, *xTD*, and xTB; (b) *yI*, *yTA*, and yTB.

Table 6
Predicted time to HP-OIT depletion (years); rounded to one significant digit.

Temp (°C)	Predicted HP-OIT depletion time (years)											
	xTDs (HP-OIT$_0$ = 1460)		*xTD* (HP-OIT$_0$ = 705)		xTB (HP-OIT$_0$ = 960)		*yI* (HP-OIT$_0$ = 780)		*yTA* (HP-OIT$_0$ = 800)		yTB (HP-OIT$_0$ = 915)	
	HP-OIT$_r$	t_d	HP-OIT$_r$	t_d	HP-OIT$_r$	t_d	HP-OIT$_r$	t_d	HP-OIT$_r$	t_d	HP-OIT$_r$	t_d
10	1183	6.7	660	3.6	934	7.1	758	14.1	777	13.5	888	11.3
15	1118	5.7	643	3.2	921	6.1	749	11.3	768	10.9	881	9.1
20	1046	4.9	622	2.8	902	5.3	737	9.2	756	8.9	872	7.4
25	968	4.3	596	2.5	875	4.6	723	7.5	741	7.3	862	6.1
30	887	3.7	564	2.2	838	4.0	704	6.1	722	6.0	849	5.0
35	804	3.2	528	1.9	792	3.5	681	5.1	698	5.0	835	4.2
40	722	2.8	487	1.7	734	3.1	653	4.2	670	4.1	819	3.5
55	498	1.9	351	1.3	512	2.1	543	2.5	557	2.5	755	2.1
65	379	1.5	265	1.0	360	1.7	453	1.8	465	1.8	702	1.5
70	328	1.4	227	0.9	294	1.5	407	1.6	417	1.6	673	1.3
75	284	1.2	192	0.9	237	1.4	361	1.4	371	1.3	642	1.1
85	213	1.0	137	0.7	149	1.1	278	1.0	285	1.0	577	0.9

-HP-OIT$_r$ = Residual HP-OIT value predicted based on sigmoidal equations in Fig. 7.
-t_d = time to HP-OIT depletion assessed based on reaching a cut-off value that is 3% of the difference between initial and residual HP-OIT values at each temperature.

antioxidant depletion times was notably smaller based on HP-OIT than on Std-OIT resulting in significantly different durations of Stage I based on the two OIT tests. Thus, the physical and mechanical properties are examined at different temperatures in the following sections to investigate the efficacy of these different antioxidants in protecting the GMB from degradation.

3.3. Melt flow index

The initial MFI was measured using the high load (HLMI-21.6 kg) and low load (LLMI-2.16 kg) melt flow index tests for all GMBs (Tables 1 and 2). All Group 1 GMBs had similar HLMI and LLMI initial values and hence texturing and adding the conductive layer did not affect the initial molecular weight of these GMBs. For Group 2 GMBs, while *yI*, *yTA*, and yTB were produced from the same resin lot, they had slightly different LLMI and HLMI values. However, given very similar HLMI results for the early aged specimens at different temperatures, the variation between the initial values could be due to the number of tests and variability in the MFI test. Thus, no notable effect of texturing and/or adding the conductive layer were evident from the initial MFI values of the different GMBs examined.

With ageing, the HLMI results of the GMBs were retained at the initial values at all temperatures below 85 °C. At 85 °C, a decrease in HLMI results was observed for all GMBs (Fig. 8) suggesting the dominance of oxidation-induced degradation by cross-linking. For all Group 1 GMBs, the onset of Stage III started after 29 months of ageing where the normalized HLMI values started to decrease and reached 60% for *xTD* and *xTC* and 55% for xTDs and xTB after 50 months of ageing. Thus, the trend of HLMI was very similar for all Group 1 GMBs (Fig. 8a) with slightly slower rate of degradation in the conductive-backed GMBs, *xTD* and *xTC*, relative to xTDs and xTB.

For Group 2 GMBs, the HLMI of yTB at 85 °C started decreasing after 15 months of ageing and this was followed by a rapid drop to 5% of the initial value by 32 months of ageing (Fig. 8b). For the conductive-backed GMBs, the normalized HLMI remained unchanged during the first 23 months for *yI* and 24 months for *yTA* and then reduced to 43% and 30% of the initial values of *yI* and *yTA*, respectively, by the end of the incubation period. Hence, the fastest HLMI degradation at 85 °C was observed for the nonconductive yTB with the shortest antioxidant depletion time followed by *yTA*, while *yI* had the slowest degradation.

While the relative degradation of *yTA* and yTB based on HLMI followed their antioxidant depletion times, the degradation of the conductive-backed and nonconductive GMBs in Group 1 (i.e., *xTD* and xTB) was very similar even though the Std-OIT depletion time of xTB was 4 months shorter than *xTD* at 85 °C (that was not related to testing method of OIT specimens as discussed in Section 3.2). This shows that the relative degradation of conductive-backed and nonconductive GMBs does not necessarily follow their relative antioxidant depletion.

3.4. Tensile properties

The tensile break properties (i.e., strength and strain) were used to investigate the thermo-oxidative degradation of the GMBs in MSW-L3. According to Zafari et al. (2023), the variation in thickness of textured GMBs can significantly increase the variation in the initial break properties. This was also evident from the higher standard deviations of tensile break strength and strain of the unaged textured xTB, *xTD*, and *yTA* relative to their smooth edges/equivalent (Tables 1 and 2). Additionally, the variation in the results increased by adding the conductive layer to the textured GMBs in both groups. For instance, the initial break strain for Type IV specimens in XD for the double-sided textured GMBs was 357 ± 175% (CoV = 49%) for *xTD*, 470 ± 120% (CoV = 25%) for xTB, 300 ± 105% (CoV = 35%) for *yTA*, and 552 ± 44% (CoV = 8%) for yTB. Thus, the conductive-backed *xTD* and *yTA* had, respectively, 2 and 4 times higher CoV than the nonconductive xTB and yTB. A similar effect of texturing in giving a high CoV relative to the smooth equivalent was also observed on specimens taken from the same samples and sent to a commercial laboratory for confirmatory testing. The higher variation in the break properties of *xTD* and *yTA* relative to xTB and yTB can be attributed to the premature failure of the conductive skin at different times from the other GMB layers in some of the specimens resulting in their delamination (Fig. 9a). This premature failure typically occurred at 30%–60% of the break elongation obtained for the specimens that did not exhibit delamination (Fig. 9b).

Delamination of the conductive layer during the tensile tests was also observed in the GMBs with smooth conductive skin (i.e., *xTC* and *yI*; Fig. 9c) that resulted in the variation of their initial break properties similar to the conductive-backed double-sided textured GMBs. However, the number of specimens from *xTC* and *yI* that showed such delamination was relatively small compared to *xTD* and *yTA*. For instance, of the 10 tensile tests performed on each of the unaged specimens of *xTD*, *xTC* and *yI*, only one *xTC* and one *yI* specimen (i.e., 10%) exhibited delamination of the conductive layer during the test compared to 4 specimens (i.e., 40%) for *xTD*. Hence, texturing increased the frequency of the delamination of the GMB multilayers.

With ageing, the tensile break strain and strength results exhibited large variation at all incubated temperatures with the data scattered around the initial values (Fig. 10). To investigate the effect of the conductive layer on the variability of the break properties using the largest possible number of samples, a new set of data was established for *xTD*, xTB, *yTA*, and yTB by combining all the break strain results for the unaged and aged specimens at different immersion temperatures below 85 °C to exclude specimens with any potential effect of the degradation on the results. Combining the results of 90 and 40 tensile tests for each of the Groups 1 and 2 GMBs, respectively, the average break strain of the new data set (mean ± standard deviation) was 399 ± 98% (CoV = 25%) for xTB, 330 ± 130% (CoV = 39%) for *xTD*, 405 ± 101% (CoV = 25%) for yTB, and 238 ± 119% (CoV = 50%) for *yTA*. Hence, prior to the oxidative degradation, the break strain of the conductive-backed GMBs

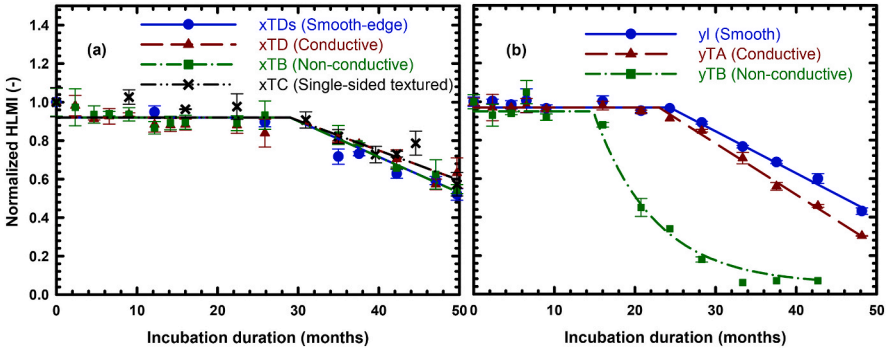

Fig. 8. Variation of normalized HLMI ($HLMI_t/HLMI_0$) with incubation duration for (a) xTDs, *xTD*, xTB, and *xTC*; (b) *yI*, *yTA*, and yTB; immersed in MSW-L3 at 85 °C.

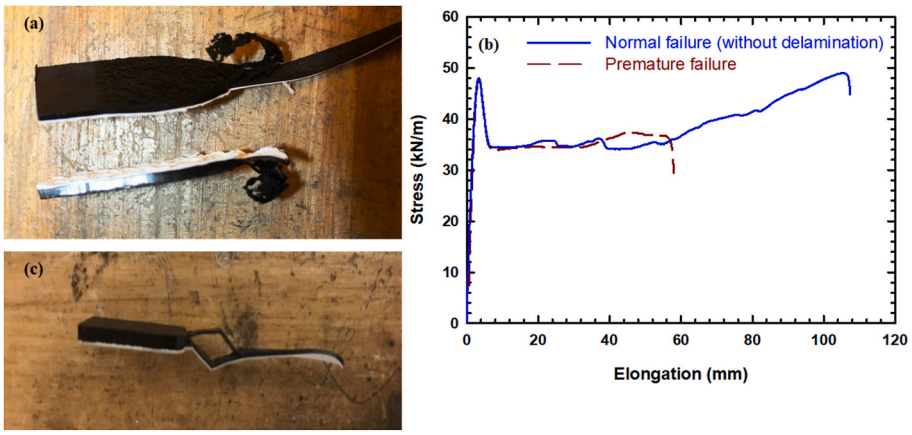

Fig. 9. (a) Failure of the tensile specimen due to separation of the conductive layer from the core layer in *xTD* specimen; (b) tensile curves for the *xTD* specimens with normal and premature failures; and (c) delamination of the conductive layer for the smooth conductive-backed *yI*.

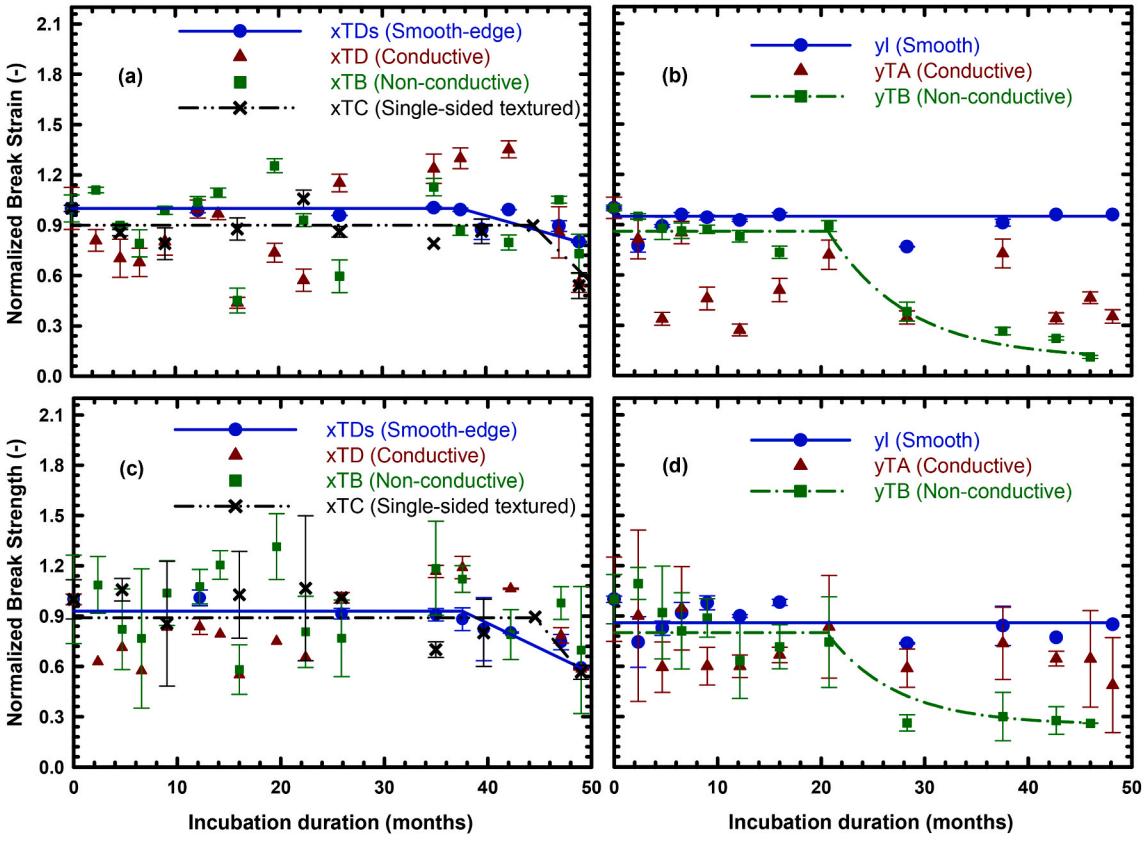

Fig. 10. Variation of (a) normalized tensile break strain in XD for xTDs, *xTD*, xTB, and *xTC*; (b) normalized tensile break strain in XD for *yI*, *yTA*, and yTB; (c) normalized tensile break strength in XD for xTDs, *xTD*, xTB, and *xTC*; (d) normalized tensile break strength in XD for *yI*, *yTA*, and yTB; after 50 months of incubation in MSW-L3 at 85 °C.

with higher CoV relative to the nonconductive GMBs was more scattered during the incubation period. Since this high variation in the results significantly complicated the assessment of polymer degradation based on break properties, the onset of thermal-oxidative degradation at 85 °C could not be deduced for xTB, *xTD*, and *yTA* during the 50 months of ageing although the degradation of these GMBs was evident based on HLMI after 29 months for xTB and *xTD* and 24 months for *yTA*. However, yTB with the lowest depletion time showed a clear reduction in the break strain after 21 months (6 months after the onset of degradation based on HLMI) and reached the time to nominal failure after 26 months of ageing at 85 °C. Thus, the tensile break properties responded slower to oxidative degradation than the HLMI and had a longer Stages II than HLMI.

Likewise, for xTDs, *xTC*, and *yI*, the time to the onset of degradation based on the tensile break properties was longer than degradation times based on HLMI. The degradation of xTDs and *xTC* based on break strength and strain at 85 °C started after 38 and 44 months, respectively (Fig. 10) but the time to nominal failure was not reached for these GMBs by the end of the data collection period. Thus, polymer degradation based on tensile break properties was faster for xTDs and *xTC* than xTD. While this may be expected for xTDs with faster Std-OIT depletion than *xTD* at 85 °C, *xTC* with the slowest depletion time in Group 1 GMBs

showed signs of polymer degradation before *xTD*. This was similar to the behaviour reported by Zafari et al. (2023) in which faster degradation based on break properties was observed for the smooth edge of the GMBs examined relative to the textured portion even when the antioxidant depletion was faster for the textured part. This implies that the greater core thickness of *xTD* may have retarded its degradation based on break properties relative to xTDs and *xTC*.

For *yI*, while no signs of degradation were observed based on break strain and strength values similar to *yTA*, the variability in the results was notably lower for the smooth *yI* than the textured *yTA*. Additionally, unlike the Group 1 GMBs, the thicker GMB yTB degraded faster than *yTA* and *yI*. This suggests that while in general thicker GMBs are expected to have longer degradation times than thinner GMBs (Rowe et al., 2010, 2014; Rowe and Ewais 2014), in conductive-backed GMBs, other factors such as the carbon black content and the distribution of carbon black can affect the degradation in their mechanical properties (Deveci et al., 2018) relative to nonconductive GMBs. The effect of these factors can be evident from the different relative performance of the conductive-backed and nonconductive GMBs in Groups 1 and 2 since they were produced by two different manufacturers with using different antioxidants/stabilizers and carbon black added to the base resin.

3.5. SCR

Early reduction in SCR values to an equilibrium stress crack resistance (SCR_m) due to physical ageing (Ewais and Rowe 2014; Rowe et al., 2019) was observed for xTDs, xTBs, *xTC*, and *yI* at all incubated temperatures while the antioxidants were still depleting and the HLMI and tensile break properties were retained at their initial values (Fig. 11). Tables 1 and 7 show the SCR_0 values obtained form testing except for xTDs which is shown as > 4000h. Three SCR tests were conducted on xTDs using the ASTM standard method and of these one is still running after 25,000h, one failed at 29,000h and one at 34,000h while SCR_m averaged about 3300h. Given the exceptionally high SCR_0 (the possible reasons are discussed below) is unexpected for this resin albeit there are three multiple values in excess of 4000h and SCR_m is around 3300h, SCR_0 is only shown as > 4000h. Excluding the 40 °C data that had not reached SCR_m during the 50 months of ageing, the effect of temperature on SCR_m values was statistically insignificant at a 95% confidence level for xTDs, xTBs, and *yI* (Table 7) showing a limited effect of the incubation temperature between 55 and 85 °C on the SCR_m. For the different smooth/single-sided textured GMBs, the average SCR_m obtained from all temperatures except for the 40 °C was 3338 ± 780h (SCR_m/SCR_0 = 11%) for xTDs, 474 ± 130h (SCR_m/SCR_0 = 29%) for xTBs, 562 ± 259h (SCR_m/SCR_0 = 37%) for *xTC*, and 1122 ± 469h (SCR_m/SCR_0 = 78%) for *yI* (Table 7). Thus, although the GMBs were manufactured using the same nominal resin, they had significantly different initial and stabilized SCR based on the ASTM use of nominal thickness to establish the notch depth.

Table 7
Values of SCR_m in hours for xTDs, xTC, and yI at different temperatures.

GMB	Mean ± Standard deviation (hours)			
	xTDs (SCR_0 > 4000)	xTBs (SCR_0 = 1630)	*xTC* (SCR_0 = 1537)	*yI* (SCR_0 = 1432)
SCR_m at 85 °C	3617 ± 1082	496 ± 129	562 ± 259	1087 ± 552
SCR_m at 75 °C	3030 ± 345	478 ± 107	N/A	N/A
SCR_m at 70 °C	N/A	N/A	N/A	1060 ± 381
SCR_m at 65 °C	3046 ± 163	467 ± 187	N/A	N/A
SCR_m at 55 °C	3306 ± 722	453 ± 107	N/A	1212 ± 438
SCR_m for data set including all obtained results at different temperatures >40 °C	3338 ± 780	474 ± 130	562 ± 259	1122 ± 469

- N/A = Not available.

The difference in the SCR values of the GMBs examined (especially between xTDs and xTBs) can be attributed to the difference in the depth of the notch applied to the SCR specimens (arising from their different actual thicknesses) and in their yield strength values (used to calculate the SCR load). For instance, the yield strength values used to calculate the SCR load for xTBs (thickness = 2.0 mm) and xTDs (thickness = 1.75

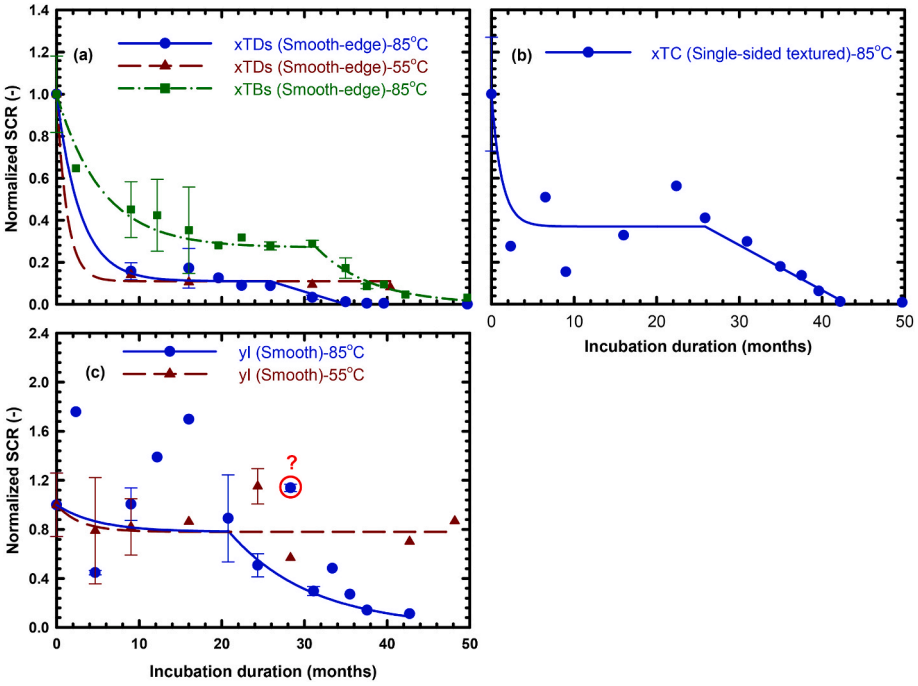

Fig. 11. Variation of normalized SCR (SCR_t/SCR_0) with incubation duration for (a) xTDs at 55 and 85 °C; (b) *xTC* at 85 °C; (c) *yI* at 55 and 85 °C; immersed in MSW-L3 (note: the degradation of the SCR below SCR_m was modelled based on experimental results to give the conservative time to nominal failure).

mm) specimens were 36 and 33kN/m, respectively. With a ligament thickness of 80% of the nominal thickness (i.e., 2.0 mm) used in notching the SCR specimens of these GMBs (per ASTM D5397 (2020b)) irrespective of their actual thickness, the cross-sectional area of the notched specimens of the different GMBs remains constant (0.8 x nominal thickness x specimen width). This results in lower tensile stresses during the SCR test for xTDs than xTBs due to its lower yield strength that may have resulted in the significantly higher initial and stabilized SCR of xTDs (SCR_0 of around 30,000h) relative to xTBs (around 1600h). Thus, following the exact procedure outlined in the current ASTM D5397 resulted in a high initial SCR value of xTDs that may not reflect the actual SCR of its base resin. This suggests that to compare the initial and stabilized SCR values of the multilayered GMBs their difference in thickness and yield strength values used to calculate the SCR load should be also considered. In addition, off-the roll specimens of different thicknesses from the same resin lot will have different residual stresses even in monolithic products due to different pulling and cooling speeds for blown-film products of different thicknesses (Rowe et al., 2019) but will have the same SCR_m. This helps explain the reduction in SCR from SCR_0 around 30,000 and 1600h to SCR_m of around 3300 and 470h for xTDs and xTBs, respectively, leaving the difference between 3300 and 470h unexplained by residual stresses and likely due to different notch depth and yield stresses used.

To investigate the effect of the notch depth in xTDs, its SCR specimens were notched to maintain a ligament thickness of exactly 80% of the actual thickness (i.e., 1.4 mm ligament instead of 1.6 mm). Because of the reduction in the ligament area, the load used for the SCR test was also reduced to maintain the same tensile stresses applied on xTBs during SCR tests. Under these conditions, the SCR_0 and SCR_m of xTDs were 5085 $\pm$ 600h and 1100 $\pm$ 60h, respectively. Although these values showed 6-fold reduction for the SCR_0 and 3-fold reduction for the SCR_m relative to the SCR values of xTDs assessed using the ASTM D5397 procedure, they were significantly higher than the values obtained for xTBs under the same tensile stresses during the SCR test. The decrease in SCR_0 from around 30,000h to around 5100h reflects the change in notch depth and tensile stress. The difference between SCR_0 and SCR_m can be explained by relaxation of residual stresses and morphological change (Rowe et al., 2019; Rowe and Ewais 2014). This leaves the different SCR_m of these two GMBs unexplained given they are said to have the nominally the same base resin, albeit from different lots. This difference in the SCR_m may in part be attributed to the difference in the SCR of different resin lots and in part due to the difference in the actual thickness of xTBs and xTDs resulting in difference in eccentricity of the tensile load applied during the SCR test. The eccentricity of the notched specimens was higher for xTBs (i.e., thicker GMB) than xTDs and hence this may have affected their SCR results.

To investigate the effect of yield strength value on the SCR degradation trend, the SCR tests were also performed for xTDs on the specimens prepared by maintaining the ligament thickness at exactly 80% of the actual thickness (i.e., 1.4 mm ligament) using the yield strength value of 36kN/m (similar to what was used for xTBs) to calculate the SCR load during the tests. Comparing these SCR results with the results obtained based on ASTM method (i.e., specimens notched at 80% of the nominal thickness and subjected to SCR load calculated based on yield value of 33kN/m) showed similar SCR degradation trend (i.e., time at which the GMB started SCR degradation and the rate of degradation in Stage III) despite the different absolute values. Thus, increasing yield strength value to calculate the SCR load had minor effect on the degradation trend and time to nominal failure defined based on a decrease to 50% of the stabilized SCR_m value. This shows that although comparing the absolute SCR values of the different multilayered GMBs can be difficult using the current ASTM method, their relative SCR degradation can be assessed by comparing their t_{NF}.

For the variability in SCR, the SCR of the conductive-backed *xTC* and *yI* exhibited a large variation relative to the nonconductive xTDs and xTBs implied by their higher CoV (23% for xTDs, 27% for xTBs, 46% for *xTC*, and 42% for *yI*) in the SCR_m results. For instance, the SCR of *yI* at 85 °C ranged between 45% and 180% of the initial SCR_0 value during the first 16 months of ageing during which the GMB did not exhibit any degradation based on HLMI and tensile properties. The large variability in the SCR of *xTC* and *yI* can be attributed to the presence of a conductive layer in the ligament of their SCR specimens that increased the non-homogeneity of the SCR specimens relative to the nonconductive GMB specimens.

While the effect of conductive layer on the SCR of the conductive-backed GMBs requires further investigation beyond what is presented in this paper, the yield strength value used to calculate the SCR load and the direction and depth of the notch applied to the SCR specimens seem to affect the results. The effect of the yield strength can be manifested if the conductive layer had different yield properties relative to the core layer and hence the yield strength value assessed for the entire thickness of the GMB may not reflect the yield strength of the core layer resisting the crack propagation in the NCTL test. However, as discussed for xTDs, the effect of these factors on the degradation trend based on SCR is considered subtle since the different aged samples were examined using a consistent approach for notching (depth and direction) and calculation of the load for the SCR test.

The degradation of the SCR beyond the SCR_m values was observed for all GMBs only at 85 °C. For the smooth edges xTDs and xTBs, the SCR started to decrease from SCR_m values at 85 °C after 26 and 31 months of ageing, respectively. With further ageing, the normalized SCR value reached 0.06% (19h) for xTDs and 3% (52h) for xTBs at the end of the incubation period. Hence, the time to nominal failure (t_{NF}) was reached after 30 and 36 months for xTDs and xTBs, respectively. This suggests that the greater thickness in xTBs (2 mm versus 1.75 mm for xTDs) may have resulted in slower degradation in xTBs relative to xTDs. Similarly, the tensile break properties of xTDs started to decrease (after 38 months) sooner than xTBs (after 42 months; Zafari et al., 2023) although their degradation based on MFI was very similar. Thus, the core thickness of xTBs and xTDs affected their relative degradation based on mechanical properties but was not evident in the MFI tests due to the complete melt of the specimens during the test.

For the specimens with conductive layer in the ligament (i.e., *yI* and *xTC*), the large variation in the SCR results complicated the assessment of the onset of polymer degradation based on SCR. For *yI*, the normalized SCR (SCR_t/SCR_0) started to decrease from the SCR_m value (78%) after 21 months then it continuously decreased to reach 11% at 43 months (Fig. 11). Thus, the t_{NF} based on SCR reaching 50% of the SCR_m was 28 months while that based on 50% of the 500h required by GRI-GM13 would be about 37 months. For *xTC*, although there was a large variation in the SCR results, a continuous decrease in the SCR values was observed after 26 months of ageing and the t_{NF} was reached after 35 and 36 months based on 50% of SCR_m and GRI-GM13's required 500h, respectively. Thus, while the presence of the conductive layer in the ligaments resulted in such high variation in SCR of *xTC* and *yI* relative to the nonconductive GMBs, the degradation of both conductive-backed GMBs was faster based on SCR than on MFI and tensile break properties.

3.6. Degradation behaviour of the multilayered GMBs at 85 °C

The length of the different degradation stages is presented for the GMBs examined in Table 8 at 85 °C since degradation beyond antioxidant depletion was not observed for all GMBs at all temperatures below 85 °C. While for all the GMBs examined the HP-OIT depletion times were longer than the Std-OIT depletion times at 85 °C, the high HP-OIT residual values retained after the initiation of polymer degradation implies that the antioxidants/stabilizers remaining after depletion to residual did not protect the GMB from oxidative degradation at 85 °C. The residual HP-OIT and time to depletion increased at lower temperatures and the time to HP-OIT depletion was less than the time to Std-OIT depletion below 75 °C. This is consistent with previous investigations that examined the degradation of HDPE GMBs stabilized with the high

Table 8
Predicted durations of the three degradation stages at 85 °C; rounded to two significant digits.

Property	xTDs	*xTD*	*xTC*	xTB	xTBs	*yI*	*yTA*	yTB
Core Thickness (mm)	1.75	2.66	2.19	2.22	2	2.38	2.20	2.36
Length of Stage I (months)								
Std-OIT	6	10	11	6	7	6	6	4
HP-OIT	13	11	12	15	16	12	12	8
Length of Stage II (months) = Time to the onset of degradation- Time to Std-OIT/HP-OIT depletion								
Break strain (XD)	32[a]/25[b]	>40[a]/>39[2]	33[a]/32[b]	>44[a]/>35[b]	35[a]/26[b]	>42[a]/>36[b]	>42[a]/>36[b]	17[a]/13[b]
SCR[c]	20[a]/13[2]	–	15[a]/14[b]	–	24[a]/15[b]	15[a]/9[b]	–	–
SCR[d]	20[a]/13[2]	–	15[a]/14[b]	–	24[a]/15[b]	15[a]/9[b]	–	–
Length of Stage III (months) = Time to 50% reduction in a property- Time to the onset of degradation								
Break strain (XD)	>12	N/A	>6	N/A	>8	N/A	N/A	5
SCR[c]	4	–	9	–	5	7	–	–
SCR[d]	10	–	10	–	5	16	–	–
Time to nominal failure (t_{NF}; in months) = Time from the start of incubation until 50% reduction in a property								
Break strain (XD)	>50	>50	>50	>50	>50	>48	>48	26
SCR[c]	30	–	35	–	36	28	–	–
SCR[d]	36	–	36	–	36	37	–	–

N/A = Not available because there were not any significant changes in the property by the end of incubation period.
[a] Based on Std-OIT depletion times.
[b] Based on HP-OIT depletion times.
[c] Time to nominal failure defined based on the SCR being reduced to 50% of the SCR_m value.
[d] Time to nominal failure defined based on the SCR being reduced to 50% of the 500 hours.

molecular weight HALS when exposed to leachates with surfactants at elevated temperatures (e.g., Ewais et al., 2014; Morsy and Rowe 2019; Zafari et al., 2023). While it is difficult to assess the effective antioxidants protecting the GMB from oxidative degradation (whether those detected by Std-OIT or by HP-OIT), degradation of all the GMBs started after their full depletion to residual values. Thus, both groups of antioxidants detected by Std-OIT and HP-OIT may have played a role in delaying oxidative degradation.

3.6.1. *Effect of conductive layer on the degradation of textured GMBs*

Comparing the performance of the nonconductive double-sided textured xTB to the conductive-backed double-sided textured *xTD* and the conductive-backed single-sided textured *xTC* shows that the Std-OIT depletion at 85 °C was longer for the two conductive-backed GMBs despite their lower initial values relative to xTB. However, the HP-OIT depletion time of xTB was longer than the two conductive GMBs. Thus, the conductive layer may have had different effects on the different antioxidants detected by Std-OIT and HP-OIT. With respect to yTB and *yTA*, while the conductive layer in *yTA* did not affect its initial OIT values relative to the nonconductive yTB, it retarded the Std-OIT depletion times resulting in longer Stage I for the conductive-backed GMB than its nonconductive counterpart. Thus, while the effect of adding the conductive layer on the length of Stage I was not particularly clear for Group 1 GMBs, the conductive-backed *yTA* depleted slower than nonconductive yTB based on both Std-and HP-OIT.

xTB, *xTC*, and *xTD* experienced a decrease in HLMI after 29 months of ageing. Thus, the differences in Std-OIT and HP-OIT depletion times did not appear to have affected the time at which HLMI began to decrease. Since the conductive-backed GMBs and the nonconductive were different in thickness, it is difficult to draw firm conclusions regarding the effect of the conductive layer on the time to change in HLMI for the Group 1 GMBs. For Group 2, while the nonconductive yTB had greater core thickness (2.36 mm) than conductive-backed *yTA* (2.2 mm), the decrease in HLMI for yTB commenced after 15 months compared to about 23–24 months for *yTA*, and hence no evidence that the conductive layer had any negative effect on the length of Stage II based on HLMI.

The length of Stage II based on tensile break strain for *xTD* and xTB was longer than *xTC* (Table 8). This shows that *xTC* had the lower retention of tensile break properties once its effective antioxidants had depleted to residual values (both Std-and HP-OIT). However, this is not necessarily related to the conductive layer in *xTC* due to its different surface texturing and core thickness relative to *xTD* and xTB. Thus, there is no evidence that the conductive layer had a major role on the degradation beyond antioxidant depletion especially that both the double-sided textured *xTD* and xTB did not exhibit any degradation in their tensile properties during the 50 months period. For Group 2, the degradation in tensile properties was substantially faster for the nonconductive yTB than *yTA*. For example, the t_{NF} of yTB based on break strain was only 26 months while degradation of *yTA* was not initiated after 48 months of ageing. Thus, the thicker GMB (i.e., yTB) degraded faster than the thinner GMB (i.e., *yTA*) that can be attributed to the effect of conductive layer added only to *yTA* (i.e., adding the conductive layer may have slowed down the degradation of the GMB).

Comparing the degradation behaviour of conductive-backed GMBs to nonconductive from both GMB groups shows that the effect of the conductive layer on the degradation behaviour may vary from one conductive-backed GMB to another. Furthermore, the degradation of these GMBs should be explored at temperatures below the 85 °C discussed herein (this will require many more years of study). This is especially important for GMBs such as *xTD* that exhibited slower depletion than xTB at 85 °C but faster depletion at lower temperatures (Tables 6 and 7) and hence the relative degradation of these GMBs may change at lower temperatures.

3.6.2. *Degradation of conductive-backed GMBs versus their smooth edge/equivalent*

Unlike the nonconductive multilayered textured GMBs examined by Zafari et al. (2023), comparing the degradation of the smooth edge and the textured part of the conductive-backed GMBs can involve differences in the formulation of the bottom skin. In this case, the relative depletion of antioxidants between the textured portion and the smooth edge can be also affected by the interaction of antioxidants with the carbon black added to the formulation of the conductive layer. While the interaction of antioxidants and carbon black can increase or decreases the rate of antioxidant depletion, the length of Stage I should be assessed by testing both parts of the roll to ensure a conservative assessment of the antioxidant depletion stage given that both the smooth edge and the

textured portion are exposed to the solution in the field.

xTD and the GMBs examined by Zafari et al. (2023) had lower core thickness at the smooth edges compared to the textured portions. Thus, the degradation of the smooth edge based on tensile properties was faster for the smooth edge than the textured portion even when the antioxidant depletion was slower for the smooth edge. In this case, a more conservative time to nominal failure can be obtained from testing the smooth edge to assess the duration of Stages II and III. Since the SCR of the double-sided textured *xTD* cannot be examined using the existing procedures of the SCR test, the effect of the different formulations of the bottom layers of *xTD* and xTDs on the SCR results is unknown. However, the SCR of the smooth edge gave the shortest time to nominal failure among all the properties examined for both portions of the roll. Hence, in the absence of evidence to the contrary, a conservative assessment of the duration of Stages II and III of conductive-backed GMBs can be obtained by testing the SCR of the smooth edge.

For *yTA* produced without smooth edges, the SCR can only be assessed using a smooth equivalent GMB (GRI-GM13, 2021). However, the smooth equivalent GMB can be either thinner or thicker than the textured GMB and hence its degradation is not necessarily faster than the textured GMB. For instance, while the thickness of *yI* (2.38 mm) was 8% greater than that of *yTA* (2.20 mm), the degradation based on HLMI of the textured *yTA* was faster than its equivalent smooth GMB *yI*. Thus, unlike *xTD* and the GMBs examined by Zafari et al. (2023), the conservative assessment of Stages II and III is not necessarily obtained by testing the smooth equivalent GMB. While for textured GMBs produced without smooth edge testing the SCR on a smooth equivalent GMB can give an idea of the quality of the base resin used in the formulation of the textured GMB, it does not represent the degradation behaviour of any part of the GMB roll in the field. This highlights the importance of relying on the degradation behaviour of the textured roll only for these GMBs and the need for establishing new testing methods to assess the SCR of the textured GMBs, especially for those that are not produced with smooth edges.

4. Conclusions

The long-term performance of three textured conductive-backed HDPE GMBs (*xTD*, *xTC*, and *yTA*) relative to their comparable textured nonconductive HDPE GMBs (xTB and yTB) was monitored in synthetic MSW leachate at a range of temperatures (40–85 °C) for 50 months to investigate the effect of the conductive layer on the performance of multilayered GMBs. To isolate the effect of texturing from the conductive layer, the performance of the smooth edge/equivalent of the conductive-backed GMBs (xTDs/*yI*) was also investigated and compared to the textured GMBs. For the test conditions and GMBs examined, the following conclusions were reached.

1. The conductive layer may antagonistically or synergistically affect the efficacy of the antioxidants stabilizing the GMB. Thus, the effect of the conductive layer on the antioxidant depletion stage may differ from one conductive-backed GMB to another depending on the antioxidant package, carbon black, and their interactions.
2. The conductive layer had a higher impact on the initial OIT and antioxidant depletion than texturing the surfaces. For instance, for the Std-OIT depletion, different early-time and later-time depletion rates and multiple exothermic peaks during the thermal oxidation were observed in one of the conductive-backed GMBs examined (*xTD*) but not in its smooth edge (xTDs) or the comparable nonconductive GMB (xTB) coming from the same manufacturer.
3. Both the incubation temperatures and the duration of the immersion tests affected the predictions of the antioxidant depletion times established using Arrhenius modelling. While faster depletion of antioxidants can be obtained using only elevated temperatures, it is also important to incubate the GMB at lower temperatures (e.g., 55 or 40 °C) to avoid inaccurate assessment of the performance of the GMB at lower field temperatures. For the effect of ageing duration, while an additional 34–41 months of ageing beyond the 9–16 months reported by Rowe et al. (2020) resulted in a longer antioxidant depletion stage for the conductive-backed and nonconductive GMBs, the deviation of the short-term predictions from the long-term predictions was higher for the conductive-backed GMBs than the nonconductive GMBs due to their complex depletion behaviour relative to nonconductive GMBs.
4. The relative degradation in the physical and mechanical properties beyond OIT depletion of the conductive-backed GMBs and their nonconductive counterparts was not always following their relative OIT depletion times. For instance, the conductive *xTC* with the longest antioxidant depletion stage among all Group 1 GMBs showed faster degradation than the nonconductive xTB. This can be attributed to the other factors that are related to the GMB manufacturing process such as the GMB core thickness, the masterbatch used for the conductive layer, and the characteristics of the carbon black in the conductive skin that can affect the degradation of conductive-backed GMBs. Thus, the durability of these GMBs should be assessed using immersion tests at different temperatures since their long-term performance cannot be explored based only on their initial properties.
5. The relative degradation of the textured multilayered GMBs to their smooth edge was affected by the core thickness of the GMBs. For textured conductive-backed and nonconductive GMBs produced with thinner smooth edges than the textured portion (e.g., *xTD* and xTB), the smooth edge consistently degraded faster than its textured counterpart. In this case, a conservative assessment of the time to nominal failure can be obtained using the smooth edges since they are part of the GMB roll exposed to the solution in the field. However, for the textured GMBs manufactured without the smooth edge (e.g., *yTA*), the thickness of the textured GMB can be either thinner or thicker than the smooth equivalent GMB made from the same formulation of the textured GMB. In this case, the assessment of the GMB degradation should only rely on the textured GMB since the smooth equivalent does not represent the degradation behaviour of any part of the GMB roll in the field.
6. The degradation in SCR of the smooth edge/equivalent was faster than the degradation of textured GMBs and their smooth edge/equivalent based on HLMI or the tensile break properties. However, a large variation was observed in the SCR results when the ligament thickness included the conductive layer that complicated the assessment of the onset of degradation based on SCR.

The outcomes of this study suggest that, at least for the conductive-backed GMBs examined, the conductive layer can increase the variability in the OIT, tensile, and SCR results that complicates the assessment of the degradation stages of the conductive-backed GMBs relative to the nonconductive GMBs. Since the OIT tests were conducted using bore-cut method, more research is required to further investigate the difference in the OIT values obtained from bore-cut samples versus homogenized samples. Additionally, both the current study and Zafari et al. (2023) showed that SCR gave the fastest degradation relative to tensile and HLMI. While SCR is only performed on the smooth edge (ASTM 2020b; GRI-GM13, 2021) or the equivalent smooth GMB made from the same formulation as the textured GMB (GRI-GM13, 2021), the thickness and outer skins of the multilayered textured conductive-backed GMBs are not necessarily the same as their smooth edges/equivalents. Thus, a new testing method is required to assess the SCR of the multilayered textured GMBs.

Data availability

Data will be made available on request.

Acknowledgments

The research presented in this paper was supported by the Natural Sciences and Engineering Council of Canada (NSERC) and the Canadian Nuclear Laboratory (CNL). The equipment used were provided by funding from the Canada Foundation for Innovation (CFI) and Ontario's Ministry of Research and Innovation.

Acronyms

ASTM	American society for testing and materials
CCL	Compacted clay liner
CoV	Coefficient of variation
CQA	Construction quality assurance
DSC	Differential scanning calorimetry
ELL	Electrical leak location
GCL	Geosynthetic clay liner
GMB	Geomembrane
HALS	Hindered amine light stabilizers
HDPE	High density polyethylene
HP-OIT	High pressure oxidative induction time
HLMI	High load melt index
LLMI	Low load melt index
MD	Machine direction
MFI	Melt flow index
MSW	Municipal solid waste
NCTL	Notched constant tensile load
OIT	Oxidative induction time
SCR	Stress crack resistance
SCR_o	Initial stress crack resistance
SCR_m	Equilibrium stress crack resistance
Std-OIT	Standard oxidative induction time
t_{NF}	Time to nominal failure
TDS	Total dissolved solids
XD	Cross-machine direction

References

Abdelaal, F.B., Rowe, R.K., 2014. Effect of high temperatures on antioxidant depletion from different HDPE geomembranes. Geotext. Geomembranes 42, 284–301.
Abdelaal, F.B., Rowe, R.K., 2017. Effect of high pH found in low-level radioactive waste leachates on the antioxidant depletion of a HDPE geomembrane. Journal of Hazardous, Toxic, and Radioactive Waste 21, D4015001.
Abdelaal, F.B., Rowe, R.K., Brachman, R.W.I., 2014a. Brittle rupture of an aged HPDE geomembrane at local gravel indentations under simulated field conditions. Geosynth. Int. 21, 1–23.
Abdelaal, F.B., Rowe, R.K., Islam, M.Z., 2014b. Effect of leachate composition on the long-term performance of a HDPE geomembrane. Geotext. Geomembranes 42, 348–362.
ASTM, 2013. Standard Test Method for Melt Flow Rates of Thermoplastics by Extrusion Plastometer D1238. American Society for Testing and Materials, West Conshohocken, Pennsylvania, USA.
ASTM, 2014. Standard Test Method for Tensile Properties of Plastics D638. American Society for Testing and Materials, West Conshohocken, Pennsylvania, USA.
ASTM, 2019. Standard Test Method for Oxidative-Induction Time of Polyolefins by Differential Scanning Calorimetry D3895. American Society for Testing and Materials, West Conshohocken, Pennsylvania, USA.
ASTM, 2020a. Standard Test Method for Determining Tensile Properties of Nonreinforced Polyethylene and Nonreinforced Flexible Polypropylene Geomembranes D6693. American Society for Testing and Materials, West Conshohocken, Pennsylvania, USA.
ASTM, 2020b. Standard Test Method for Evaluation of Stress Crack Resistance of Polyolefin Geomembranes Using Notched Constant Tensile Load Test D5397. American Society for Testing and Materials, West Conshohocken, Pennsylvania, USA.
ASTM, 2020c. Standard Test Method for Oxidative Induction Time of Polyolefin Geosynthetics by High-Pressure Differential Scanning Calorimetry D5885. American Society for Testing and Materials, West Conshohocken, Pennsylvania, USA.
ASTM, 2021a. Standard Test Method for Oxidative Induction Time of Polyolefin Geosynthetics by Differential Scanning Calorimetry D8117. American Society for Testing and Materials, West Conshohocken, Pennsylvania, USA.
ASTM, 2021b. Standard Guide for Selection of Techniques for Electrical Leak Location of Leaks in Geomembranes D6747. American Society for Testing and Materials, West Conshohocken, Pennsylvania, USA.
Charpentier, C., Jacquelin, T., 2018. In-depth comparison of exposed geomembrane leak location methods. In: International Conference on Geosynthetics (Seoul, South Korea).
Deveci, S., Antony, N., Eryigit, B., 2018. Effect of carbon black distribution on the properties of polyethylene pipes-Part 1: degradation of post yield mechanical properties and fracture surface analyses. Polym. Degrad. Stabil. 148, 75–85.
Ewais, A.M.R., Rowe, R.K., 2014. Effect of aging on the stress crack resistance of an HDPE geomembrane. Polym. Degrad. Stabil. 109, 194–208.
Ewais, A.M.R., Rowe, R.K., Brachman, R.W.I., Arnepalli, D.N., 2014. Service life of a high-density polyethylene geomembrane under simulated landfill conditions at 85°C. J. Geotech. Geoenviron. Eng. 140, 04014060.
Forget, B., Rollin, A., Jacquelin, T., 2005. Impacts and Limitations of Quality Assurance on Geomembrane Integrity. Sardinia's.
Gholami, F., Pircheraghi, G., Sarafpour, A., 2020. Long-term mechanical performance of polyethylene pipe materials in presence of carbon black masterbatch with different carriers. Polym. Test. 91, 106857.
Gilson-Beck, A., 2019. Controlling leakage through installed geomembranes using electrical leak location. Geotext. Geomembranes 47, 697–710.
Giroud, J.P., Bonaparte, R., 1989. Leakage through liners constructed with geomembranes—part I. Geomembrane liners. Geotext. Geomembranes 8, 27–67.
Gri-GM13, 2021. Standard Specification for Test Methods, Test Properties, and Testing Frequency for High Density Polyethylene (HDPE) Smooth and Textured Geomembranes. Geosynthetic Research Institute, PA, USA.
Hawkins, W.L., Hansen, R.H., Matreyek, W., Winslow, F.H., 1959. The effect of carbon black on thermal antioxidants for polyethylene. Rubber Chem. Technol. 32, 1164–1170.
Hsuan, Y., Schroeder, H., Rowe, K., Müller, W., Greenwood, J., Cazzuffi, D., Koerner, R., 2008. Long-term performance and lifetime prediction of geosynthetics. In: Proceedings of the 4th European Conference on Geosynthetics (Edinburgh, September. Keynote paper).
Hsuan, Y.G., Koerner, R.M., 1998. Antioxidant depletion lifetime in high density polyethylene geomembranes. J. Geotech. Geoenviron. Eng. 124, 532–541.
Huang, J.-C., 2002. Carbon black filled conducting polymers and polymer blends. Adv. Polym. Technol. 21, 299–313.
Koerner, R.M., 2012. Designing with Geosynthetics. Xlibris Corporation.
Koerner, R.M., Lord, A.E., Hsuan, Y.H., 1992. Arrhenius modeling to predict geosynthetic degradation. Geotext. Geomembranes 11, 151–183.
Kovács, E., Wolkober, Z., 1976. The effect of the chemical and physical properties of carbon black on the thermal and photooxidation of polyethylene. J. Polym. Sci., Polym. Symp. 57, 171–180.
Messmer, D.P., Cadwallader, M., 1994. Improved geomembrane damage/leak detection through co-extrusion technology. Waste Age 25, 213–222.
Morsy, M., Rowe, R.K., 2019. Effect of texturing on the longevity of HDPE geomembranes in municipal solid waste landfills. Can. Geotech. J.
Mueller, W., Jakob, I., 2003. Oxidative resistance of high-density polyethylene geomembranes. Polym. Degrad. Stabil. 79, 161–172.
Mwila, J., Miraftab, M., Horrocks, A.R., 1994. Effect of carbon black on the oxidation of polyolefins—an overview. Polym. Degrad. Stabil. 44, 351–356.
Ng, H., Zheng, Y., 2016. Electrically Conductive Geomembrane Enhances Construction Quality Assurance at Post Installation, 2. Japanese Geotechnical Society Special Publication, pp. 2401–2405.
Pantea, D., Darmstadt, H., Kaliaguine, S., Roy, C., 2003. Electrical conductivity of conductive carbon blacks: influence of surface chemistry and topology. Appl. Surf. Sci. 217, 181–193.
Peña, J.M., Allen, N.S., Edge, M., Liauw, C.M., Roberts, I., Valange, B., 2000a. Triplet quenching and antioxidant effect of several carbon black grades in the photodegradation of LDPE doped with benzophenone as a photosensitiser. Polym. Degrad. Stabil. 70, 437–454.
Peña, J.M., Allen, N.S., Edge, M., Liauw, C.M., Valange, B., 2001a. Interactions between carbon black and stabilisers in LDPE thermal oxidation. Polym. Degrad. Stabil. 72, 163–174.
Peña, J.M., Allen, N.S., Edge, M., Liauw, C.M., Valange, B., 2001b. Studies of synergism between carbon black and stabilisers in LDPE photodegradation. Polym. Degrad. Stabil. 72, 259–270.
Peña, J.M., Allen, N.S., Liauw, C.M., Edge, M., Valange, B., 2000b. Factors influencing the adsorption of stabilizers onto carbon black: flow microcalorimetry studies. J. Vinyl Addit. Technol. 6, 62–68.
Phease, T.L., Billingham, N.C., Bigger, S.W., 2000. The effect of carbon black on the oxidative induction time of medium-density polyethylene. Polymer 41, 9123–9130.
Priyanto, D., Whitelaw, B., Rowe, R., Barone, F., Abdelaal, F., Zafari, M., Buckley, J., 2019. Implementation of Research and Development (R&D) Results in the Design of Liner System for the Near Surface Disposal Facility (NSDF)–19089. WM2019 Conference. March, pp. 3–7.
Rowe, R.K., 2005. Long-term performance of contaminant barrier systems. Geotechnique 55, 631–678.
Rowe, R.K., 2020. Protecting the environment with geosynthetics: 53rd karl terzaghi lecture. J. Geotech. Geoenviron. Eng. 146, 04020081. Rowe, R.K., Abdelaal, F.B. & Brachman, R.W.I. 2013. Antioxidant depletion of HDPE geomembrane with sand protection layer. Geosynthetics International, 20(2): 73-89.
Rowe, R.K., Abdelaal, F.B., Islam, M.Z., 2014. Aging of high-density polyethylene geomembranes of three different thicknesses. J. Geotech. Geoenviron. Eng. 140, 04014005.
Rowe, R.K., Abdelaal, F.B., Zafari, M., Morsy, M.S., Priyanto, D., 2020. An approach to HDPE geomembrane selection for challenging design requirements. Can. Geotech. J.
Rowe, R.K., Islam, M.Z., Hsuan, Y.G., 2010. Effects of thickness on the aging of HDPE geomembranes. J. Geotech. Geoenviron. Eng. 136, 299–309.

Rowe, R.K., Jefferis, S., 2022. Protecting the environment from contamination with barrier systems: advances and challenges. In: Proceedings of the 20th International Conference on Soil Mechanics and Geotechnical Engineering (Sydney, Australia).
Rowe, R.K., Ewais, A.M.R., 2014. Antioxidant depletion from five geomembranes of same resin but of different thicknesses immersed in leachate. Geotext. Geomembranes 42, 540–554.
Rowe, R.K., Islam, M.Z., Hsuan, Y.G., 2008. Leachate chemical composition effects on OIT depletion in an HDPE geomembrane. Geosynth. Int. 15, 136–151.
Rowe, R.K., Morsy, M.S., Ewais, A.M.R., 2019. Representative stress crack resistance of polyolefin geomembranes used in waste management. Waste Manag. 100, 18–27.
Rowe, R.K., Quigley, R.M., Brachman, R.W.I., Booker, J.R., 2004. Barrier Systems for Waste Disposal Facilities, 2nd. Spon Press, New York, USA.
Rowe, R.K., Rimal, S., Sangam, H., 2009. Ageing of HDPE Geomembrane Exposed to Air, Water and Leachate at Different Temperatures, 27. Geotextiles and Geomembranes, pp. 137–151.
Rowe, R.K., Sangam, H.P., 2002. Durability of HDPE geomembranes. Geotext. Geomembranes 20, 77–95.
Sangam, H.P., Rowe, R.K., 2002. Effects of exposure conditions on the depletion of antioxidants from high-density polyethylene (HDPE) geomembranes. Can. Geotech. J. 39, 1221–1230.
Scheirs, J., 2009. A Guide to Polymeric Geomembranes: a Practical Approach. John Wiley & Sons.
Scheirs, J., Marta, A.L., Armstrong, C.J., Jotani, R., 2020. Rapid Screening Test for Assessing Durability of Geomembranes in Mining Liquors. GeoAmericas, Rio De Janeiro, Brazil.
Spahr, M.E., Gilardi, R., Bonacchi, D., 2017. Carbon black for electrically conductive polymer applications. In: ROTHON, R. (Ed.), Fillers for Polymer Applications. Springer International Publishing, Cham.
Touze-Foltz, N., Bannour, H., Barral, C., Stoltz, G., 2016. A review of the performance of geosynthetics for environmental protection. Geotext. Geomembranes 44, 656–672.
Wong, W.-K., Hsuan, Y.G., 2012. Interaction between carbon black and antioxidants in high-density polyethylene pipe resin. Transport. Res. Rec. 2310, 137–144.
Wong, W.-K., Hsuan, Y.G., 2014. Interaction of antioxidants with carbon black in polyethylene using oxidative induction time methods. Geotext. Geomembranes 42, 641–647.
Wong, W.-K., Hsuan, Y.G., 2016. Effects of carbon black on the depletion of antioxidants in HDPE under air and water conditions. In: Geosynthetics, Forging a Path to Bona Fide Engineering Materials. Honoring, pp. 61–71.
Zafari, M., Abdelaal, F.B., Rowe, R.K., 2023. Degradation behavior of two multilayered textured white HDPE geomembranes and their smooth edges. J. Geotech. Geoenviron. Eng. 149, 04023020.